Ore Geology Reviews 128 (2021) 103923

Contents lists available at ScienceDirect

Ore Geology Reviews

journal homepage: www.elsevier.com/locate/oregeorev

Petrogenesis of Neoproterozoic rare metal granite-pegmatite suite in Jiangnan Orogen and its implications for rare metal mineralization of peraluminous rock in South China

Zheng-Hang Lv [a,*], Juan Chen [b], Hui Zhang [a,*], Yong Tang [a]

[a] Key Laboratory of High-Temperature and High-Pressure Study of the Earth's Interior, Institute of Geochemistry, Chinese Academy Sciences, Guiyang 550081, China
[b] School of Chemical Engineering, Guizhou Institute of Technology, Guiyang 550003, China

ARTICLE INFO

Keywords:
Petrogenesis
Neoproterozoic
Rare metals
Pegmatite
Jiangnan Orogen

ABSTRACT

Recent studies have demonstrated the Mesozoic explosive metallogeny of rare metals in China; however, Precambrian rare metal mineralization event is rarely reported or studied. The Jiangnan Orogen (JO) is a well-preserved Neoproterozoic orogenic belt in South China, and although it abounds with a huge amount of Neoproterozoic granitoids, lacks the equivalent amount granitic pegmatite. In this study, the geology, mineralogy, whole-rock composition, zircon U-Pb age and Hf isotope compositions of the Fanjingshan granite and surrounding rare metal pegmatites, and bulk composition of sedimentary wall rocks of the Taojinhe Formation in Guizhou province, western Jiangnan Orogen (JO), were studied to reveal the petrogenesis of the granite and pegmatite and the source relationship of the pegmatite with the Paleozoic and Mesozoic rare metal ore deposits in South China. The Fanjingshan granite and pegmatite both show Sn-Ta-Nb mineralization and have consistent zircon U-Pb ages of ca. 830 Ma, indicating the existence of the Neoproterozoic rare metal granite-pegmatite suite in the JO. The geology, mineralogy, whole-rock composition and zircon U-Pb age and Hf isotope study results demonstrate that the Fanjingshan rare metal pegmatite belongs to the Li-P-B-Sn-Ta-Nb granitic pegmatite in the Chemical composition-Mineral assemblage-Structural geology (CMS) classification (Dill, 2016), and has close spatial–temporal and source-differentiation connections with the Fanjingshan granite. The petrography and whole-rock composition studies revealed that the Taojinhe formation was formed by the deposition of mature and immature source materials from acidic igneous rocks in a continental arc setting. Comparison of the Hf isotope compositions of the Fangjingshan granite-pegmatite suite with those of the Fangjinshan Group and the high Li, Sn, Rb, W, Ta and Nb background concentrations in the Taojinhe Formation support the conclusion that the Taojinhe Formation was a contributing source to the granite-pegmatite suite. A comparative study of the Fanjingshan granite with synchronous S-type granitoids revealed that the granitoids in the eastern and western JO have distinct sources and degrees of differentiation, indicating the limited ore-forming potential of the Neoproterozoic granitoids in the eastern JO. The Fanjingshan rare-metal granite-pegmatite suite has consistent Hf isotope model ages of 1.6–2.3 Ga with the Paleozoic and Mesozoic Nb-Ta ± Sn-W ± Be-Li ore deposits in South China, indicating a common origin from the Paleoproterozoic crust and the source inheritance of the western JO from the Cathaysia Block.

1. Introduction

Recently, rare metals including Li, Be, Ta, Nb, Rb and Cs have been listed in the Critical Metal Catalogue by China, the European Union and the United States (Zhai et al., 2019); this inspired research interest in rare metal granites and pegmatites and strong concern in the international market regarding resource rates. As one of the dominant rock types for rare metal production, granitic pegmatites (hereafter referred to as pegmatite) are habitually attributed to the derivatives of granitic melts by several geologists. However, in the classification of pegmatite (Černý, 1991; Černý and Ercit, 2005), the abyssal and muscovite classes of pegmatite have been distinguished from other granite-related pegmatites. The abyssal pegmatites are associated with high-grade metamorphism (upper amphibolites to low- and high-P granulite facies), and

* Corresponding authors.
E-mail addresses: lvzhenghang@vip.gyig.ac.cn (Z.-H. Lv), zhanghui@vip.gyig.ac.cn (H. Zhang).

https://doi.org/10.1016/j.oregeorev.2020.103923
Received 15 July 2020; Received in revised form 27 November 2020; Accepted 5 December 2020
Available online 9 December 2020

show mineralization of rare earth elements (REEs), U, Th, Ti, Zr, and Be in some cases (e.g., (Černý and Ercit, 2005). In recent years, abundant rare metal pegmatites have been suggested to form via anatexis (e.g., (Dill, 2015a, 2015b, 2016; Shaw et al., 2016; Simmons and Falster, 2016; Müller et al., 2017; Lv et al., 2018). Some of the anatectic pegmatites are identical to the abyssal pegmatites with regard to origin, geology and mineralization, and some are different due to the presence of Li-aluminosilicates. Therefore, petrogenesis is a critical aspect in the study of pegmatite, because it controls the mineralization type of pegmatite and helps prospect rare metal ore deposits in pegmatites.

Rare metal pegmatite formation is mostly associated with continental orogeny. The thickened continental crust, crust-mantle interaction and post-tectonic extension during orogeny are beneficial to pegmatite formation (e.g., (Černý, 1991; Černý et al., 2012a; Lv et al., 2012, 2018; Zagorsky et al., 2014; Dill, 2015; Müller et al., 2017). For granite-related pegmatites, the Li-, Cs- and Ta-rich pegmatites are controlled by S-type granites originated from the partial melting of sedimentary rocks during the late- to post-orogenic stage. The Nb-, Y- and F-rich pegmatites are associated with A-type granites ('A' denotes anorogenic only) derived from granulites present deep in the continental crust or mantle magma during the post-orogenic stage or in the anorogenic rift zone (e.g., (Černý et al., 2012a). For the anatectic pegmatites, they show correlations with regional tectonothermal or high-grade metamorphic events during orogeny (e.g., Dill, 2015a, 2015b; Shaw et al., 2016; Müller et al., 2017; Lv et al., 2018). Recent statistics on the formation times of rare metal pegmatites worldwide demonstrate the temporal coupling of pegmatite formation with supercontinent assembly (Tkachev, 2011; McCauley and Bradley, 2014).

In China, pegmatites are widely distributed in various orogens (including those after cratonization) with formation times ranging from Neoarchean to Neogene (Hou, 2018). Recent studies have revealed that the predominant rare metal pegmatites and their associated large to super-large ore deposits were synchronously formed in Triassic. These include the Koktokay No. 3 pegmatite with large Be-Li-Ta-Nb-Cs ore deposits and the Kaluan pegmatites with large Li ore deposits in the Altai Orogen (220–211 Ma, Wang et al., 2007; Ma et al., 2015), the Jiajika pegmatites with super-large Li ore deposits in the Songpan-Ganzi Orogen (223–214 Ma, Hao et al., 2015) and the Bailongshan-Dahongliutan pegmatites with superlarge Li-Rb ore deposit in the West Kunlun Orogen (218–212 Ma, Yan et al., 2018). The Triassic explosive generation of pegmatite and metallogeny of rare metals probably associate with the pervasive Triassic orogeny in China. Comparatively, the Precambrian rare metal pegmatites are rarely found or studied. The Jiangnan Orogen (JO), a well-preserved Precambrain orogen in South China, was formed via the amalgamation of the Yangtze and Cathaysia blocks during the early Neoproterozoic (e.g., Shu et al., 2006; Zhao et al., 2011; Wang et al., 2017; Yao et al., 2019). Although granitic rocks are highly exposed in the orogen and have been studied extensively (e.g., (Li et al., 2003; Wang et al., 2004, 2006, 2014; Zheng et al., 2007, 2008; Yao et al., 2014), their equivalent pegmatites are very rare and negligible attention has been given to their petrogenesis and mineralization. In this study, the geology, mineralogy, bulk composition, zircon U-Pb age and Hf isotope of the Fanjingshan granite and surrounding pegmatites, and the bulk composition of the sedimentary wall rocks of the granite and pegmatites in Guizhou province, western Jiangnan Orogen, were studied to reveal the petrogenesis of the granite and pegmatites. Additionally, this study aims to evaluate the ore-forming potential of the Neoproterozoic granitoids in the orogen, and to reveal the source of rare metal ore deposits of peraluminous rock in South China.

2. Geology setting

2.1. Geology of Jiangnan Orogen

The JO is located in northwest of the Cathaysia Block and southeast of the Yangtze Block, and extends from northern Guangxi to northern of Zhejiang Province with a holistic NEE strike (strikelength of ca. 1500 km and width range of 100–200 km). It is bounded by the Jiangshan-Shaoxing and Jiujiang-Shaitai faultS to the southeast and northwest, respectly (Wang et al., 2017) (Fig. 1). The sedimentary formations, ophiolites, and volcanic and metamorphic rocks show diversities between the eastern and western sections of the JO. The sedimentary formations include the early (Sibao and equivalent groups) and late (Banxi and equivalent groups) Neoproterozoic strata (Fig. 1), with an unconformable contact relationship between them (e.g., BGMRGXP, 1985; BGMRGZP, 1987). As the fold basement in the JO, the former has been suggested to deposit in a back-arc setting during ca. 820–870 Ma and has diverse sources in the eastern and western segments (e.g., Wang et al., 2014; Li et al., 2016; Yao et al., 2019). The ophiolites show linear exposure along the northeast Jiangxi fault (Fig. 1), and the exposed ophiolites in the northeastern part of the Jiangxi Province and southern part of the Anhui Province have diverse whole-rock compositions and formation ages of 1035–970 Ma (e.g., Li et al., 1994; Gao et al., 2009; Sun et al., 2017) and 846–826 Ma (e.g., Yin et al., 2013; Zhang et al., 2013), respectively, and have been suggested to form at the forearc and backarc basin settings, respectively. Although similar ophiolites have been not confirmed in the western segment, the mafic–ultramafic rocks exposed in North Guangxi province have recently been considered part of the ophiolitic mélange (Yao et al., 2016). Arc volcanic rocks are typical in the eastern segment and are represented by tuff, basalt, andesite, spilite, dacite and rhyolite in Shuangwuxi Group (e.g., (Yang et al., 2009)with ages ranging from 930 to 880 Ma (e.g., Cheng, 1993; Li et al., 2009). Similar rock associations have not been found in the western segment to date, instead of the local exposure of high-Mg basalt in northern Guangxi (Zhao and Zhou, 2013). The regional metamorphism in the JO is poorly known due to the lack of sufficient constraints on the grade and scale of the metamorphic rock. The Neoproterozoic strata in the JO are pervasively characterized by low-grade greenschist, and amphibolite facies metamorphism has been observed only in the Lushanxingzi Group, located in northern Jiangxi Province (e.g., (Wu et al., 1998). Additionally, a few of high-pressure metamorphic rocks such as glaucophane and jadeite-albite schists, have been observed in the exposed ophiolites in northeast Jiangxi Province (Shu et al., 1994). The general absence of regional high-grade metamorphism in the Neoproterozoic strata was therefore interpreted by a location far away from the collision zone (Wang et al., 2017) or a reduction in the stress effect caused by bidirectional subduction (Zhao, 2015).

Granitoids are predominant igneous rocks in the JO and hosted by the Neoproterozoic sedimentary-metamorphic basement sequences (Fig. 1). According to previous statistics, the exposed granitoid areas are 1800 km^2 and 5000 km^2 in the western and eastern segments of the JO, respectively (Wang et al., 2017). They are primarily composed of granodiorite and monzonitic granite, they also contain small amounts of dacite, two-mica granite and leucogranite, and are mostly S-type granitoids (e.g., Li et al., 2003; Wang et al., 2004, 2006, 2014; Zheng et al., 2007, 2008; Yao et al., 2014). The granitoids have two dominat age groups of 835–800 Ma and 800–750 Ma, and are suggested to form during the post-orogenic stage and under a continental rifting setting, respectively (e.g., Zheng et al., 2007). Although the Neoproterozoic granitoids are prevalent in the JO, the synchronous pegmatite presence is nominal.

Recent tectonic-magmatic-sedimentary studies have demonstrated that the JO was formed via Neoproterozoic orogeny later than the typical Grenvillian orogenic event. The JO is a typical accretion-type orogenic belt formed after ocean-ocean subduction (ca. 880–970 Ma), arc-continent collision (ca. 860–880 Ma), ocean-continent subduction (ca. 830–860 Ma), and post-orogenic extension (ca. 800–830 Ma) (Zhao et al., 2011; Wang et al., 2014, 2017; Yao et al., 2019).

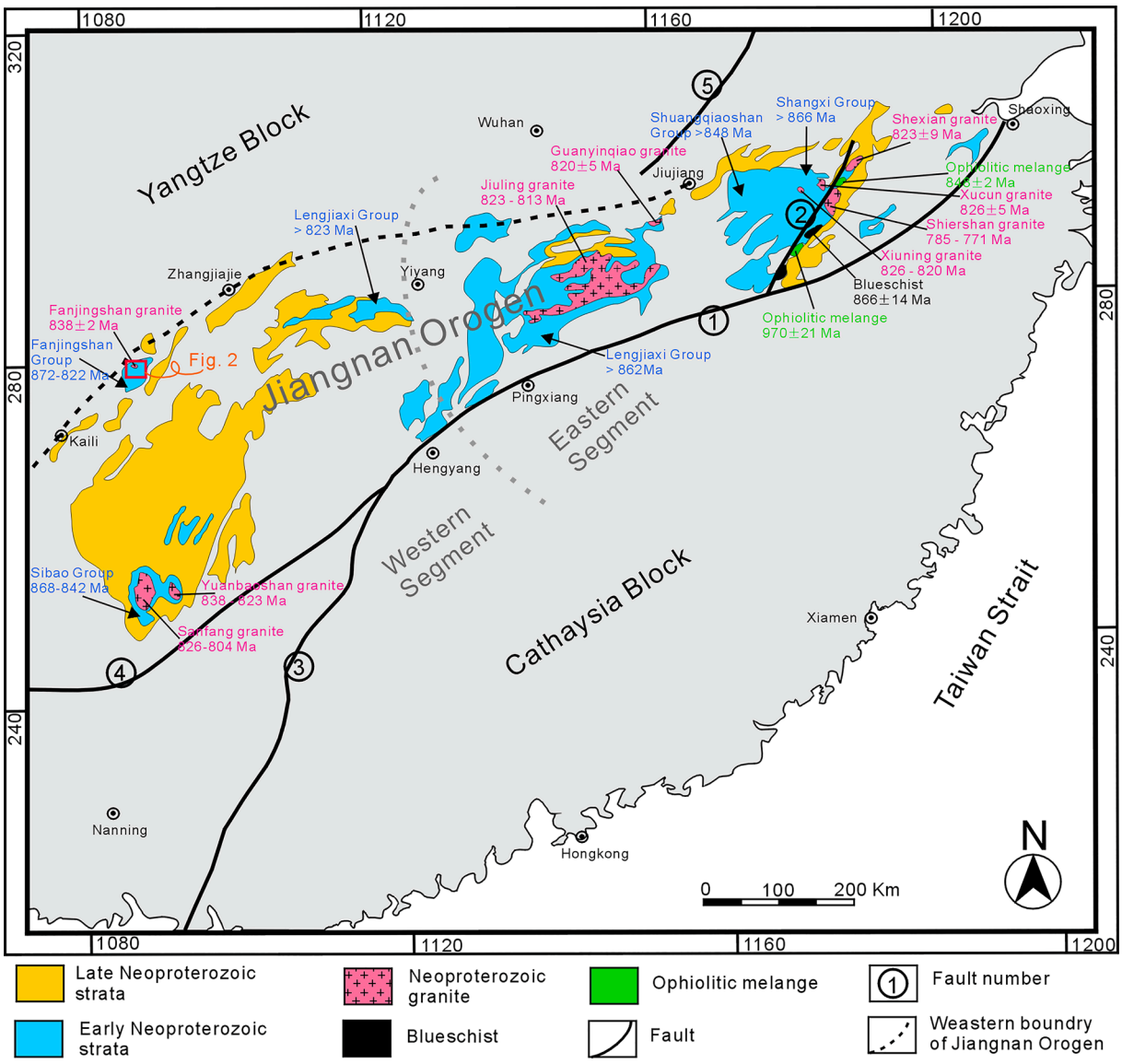

Fig. 1. Geological sketch map of the Jiangnan Orogen in South China (modified after (Yao et al., 2014) and (Zhao and Cawood, 2012). The regional faults include (1) Jiangshan - Shaoxing fault, (2) Northeast Jiangxi fault, (2) Chenzhou-Linwu fault, (4) Shizong-Mile-Luodian fault and (5) Tanlu fault.

2.2. Geology of Fanjingshan mining area

The Fanjingshan mining area is located in northeastern Guizhou, in the southwest portion of the JO. Tectonically, it is located in the axis region of the Zhangjiayan anticline, which is intersected by the Taojinhe Fault and secondary faults (Fig. 2). Sedimentary rocks are widely exposed and primarily include the lower Fanjingshan Group, i.e., the Taojinhe, Yujiagou and Xiaojiahe Formations, which are unconformably overlain by the Banxi Group. The lower Fanjingshan Group is mainly composed of epimetamorphic tuff, sandstone, siltstone, slate and phyllite, with abundant mafic volcanic interlayers (BGMRGZP, 1987). Several muscovite granite stocks are sporadically exposed in the Taoshulin, Mocaogou, Zhangjiayan and Taojinhe areas, and intruded in the Taojinhe and Yujiagou Formations. Pegmatite dykes are predominantly distributed around the Taoshulin and Mocaogou granites and intruded in the Taojinhe Formation. In the Taojinhe area, a few of small pegmatites were observed in the Taojinhe granite (Fig. 2). According to previous works, the volcanic rocks and granite exposed in Taoshulin area have zircon U-Pb ages of ca. 850 Ma and 830 Ma, respectively (Wang et al., 2011, 2016; Zhao et al., 2011) . In addition, the U-Pb chronology study of detrital zircon revealed a maximum depositional age of ca. 870 Ma for the Fanjingshan Group (e.g., Zhou et al., 2009).

2.3. Geology of the Fanjingshan granite

The Fanjingshan granite primarily consists of Taoshulin, Mocaogou, Zhangjiayan and Taojinhe granite stocks (Fig. 2), which have similar in lithofacies and different colors due to their tourmaline contents. They are mainly composed of quartz, microcline, albite, muscovite, and schorl (Table 1) and are categorized as muscovite granite (Fig. 3a). Albitization and greisenization are locally observed in the outcrops of the stocks and have increased grades upward. Microclines generally show the occurrence of pseudomorphs due to the replacement of albite. Moreover, abundant pegmatitic tourmaline-quartz schlierens were also observed. In Pit No. 209 of the Taoshulin area, several aplitic-pegmatitic veins traced to the Taoshulin granite, with mineral grain sizes varying from aplitic to pegmatitic with distance (BGGZP, 1962). According to an early geological survey, the stocks are believed to connect to the same batholith at lower depths (BGGZP, 1962).

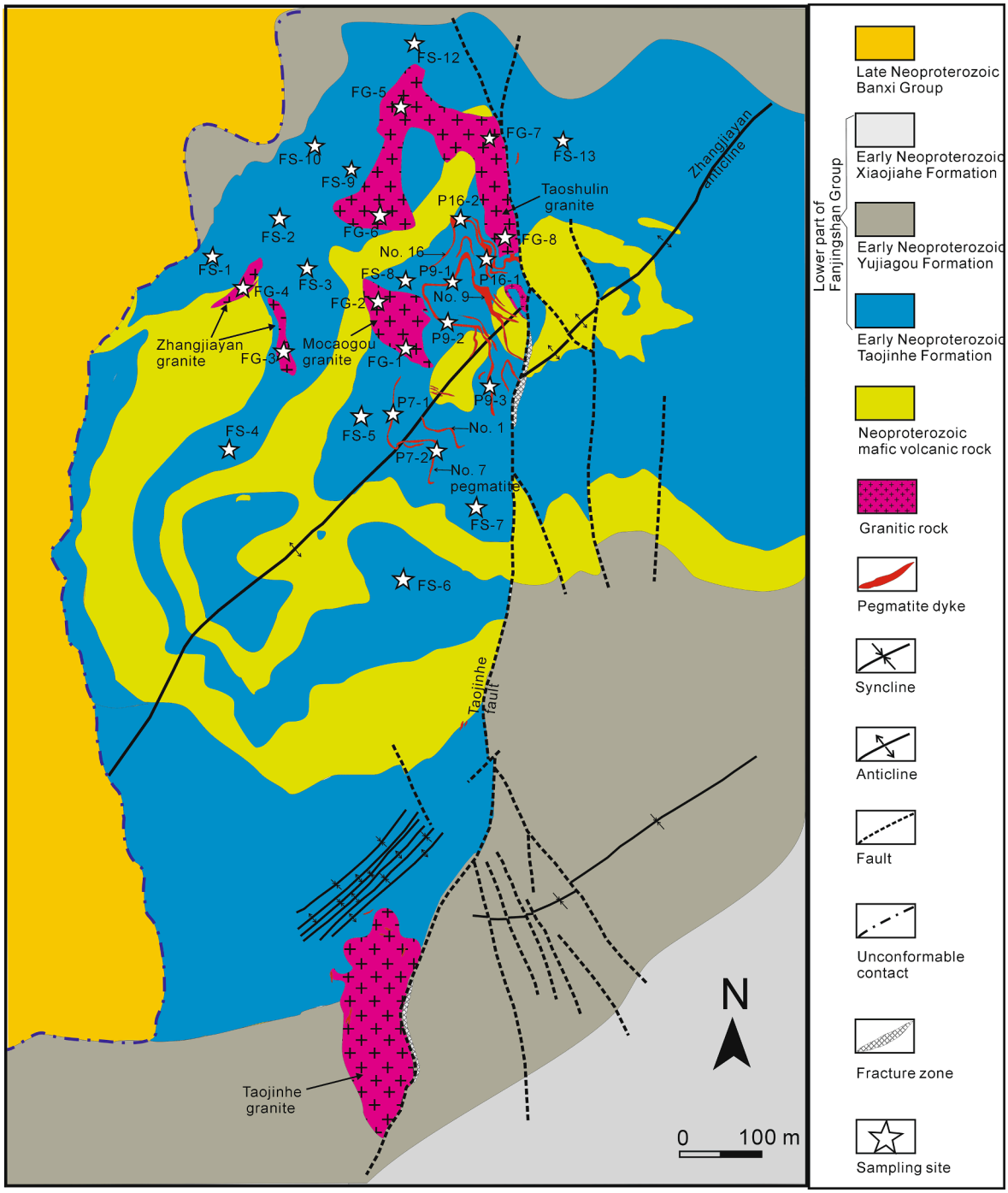

Fig. 2. Geological map of the Fanjingshan mining area and sampling locations (modified after BGGZP, 1962).

2.4. Geology of the Fanjingshan pegmatite

Twenty-one pegmatite dykes were marked by a previous geological survey (BGGZP, 1962), which are predominantly distributed in the *exo*-contact zone of the granite; these dykes mostly have simple internal zonation and limited mineralization grade. Four pegmatite dykes, including the Nos. 1, 7, 9 and 16, show larger scale and evident rare metal mineralization. The No. 7 pegmatite intruded in the slates of the Taojinhe Formation and consists of three branch veins, numbered 7–1, 7–2 and 7–3 (Fig. 2). They show tabular shapes with lengths about 510 m, 270 m and 140 m, respectively, with a maximum thickness of 4.2 m. The three branch veins contain similar rock-forming minerals and are characterized by diverse internal zoning and mineralization. Among them, the No. 7–3 branch vein has the most intensive internal zoning and mineralization, in which aplitic rim zone (0.2–0.5 m thickness), coarse feldspar-quartz-muscovite intermediate zone (0.5–1 m thickness) and blocky feldspar-quartz core zone (0.2–0.5 m thickness) were developed. In the rim and intermediate zones, albitization and muscovitization are common and are accompanied by the occurrence of columbite-Mn, tantalite-Mn, cassiterite, and microlite minerals, with Nb and Ta abundances >0.02% (BGGZP, 1962). The No. 7–2 branch vein has similar internal zoning and ore minerals as those of the No. 7–3 branch vein; three internal zones with gradual contact and constant thicknesses were observed in the outcrop (Fig. 3c). Albitization and sericitization are mostly developed in the expansion part and are accompanied by Sn-Ta-Nb mineralization. Comparatively, the No. 7–1

Table 1
The mineral assemblages of the Fanjingshan granite and pegmatite from the western Jiangnan Orogen

Pegmatite and granite		No. 7 pegmatite			No. 9 pegmatite			No.16 pegmatite			Mocaogou granite	Zhangjiayan granite	Taoshulin granite
Samples		FP7-1 and FP7-2			FP9-1 to FP9-3			FP16-1 and FP16-2			FG-1 and FG-2	FG-3 and FG-4	FG-5 to FG-8
Internal zone (Vol%)		RZ (40%)	IZ (40%)	CZ (20%)	RZ (30%)	IZ (55%)	CZ (15%)	RZ (50%)	IZ (40%)	CZ (10%)	None	None	None
Rock-forming mineral	Quartz	30–33%	30–35%	60–70%	30–33%	35–40%	50–60%	30–35%	40–45%	50–55%	30–35%	30–33%	30–40%
	Microcline	25–30%	20–25%	20–30%	20–25%	20–25%	30–35%	20–25%	15–20%	25–30%	20–25%	20–25%	20–30%
	Muscovite	20–25%	15–20%	5–10%	25–30%	15–20%	5–8%	15–20%	15–20%	3–6%	15–20%	20–25%	15–25%
	Albite	15–20%	20–25%	5–10%	20–25%	25–30%	5–10%	25–30%	20–25%	10–15%	25–30%	20–25%	25–30%
	Schorl	2%	3%	5%	3%	2%	3%	2%	2%	3%	3%	3%	3–5%
Ore mineral	Columbite-(Fe)	–	–	–	–	–	–	–	–	–	++	++	++
	Columbite-(Mn)	++	+++	+	++	+++	–	+	++	–	–	–	–
	Cassiterite	++	++	–	++	++	–	+	+	–	+	+	+
	Microlite	+	+	+	–	+	+	–	–	+	–	–	–
	Lepidolite	+	++	+	++	++	+	+	+	+	–	–	–
	Tantalite-(Mn)	–	+	+	–	–	–	–	–	–	–	–	–
	Thoreaulite	+	+	–	–	+	–	–	–	–	–	–	–
Accessory mineral	Apatite	+++	++	+	++	+++	+	++	+++	+	++	++	++
	Spessartite	++	++	++	++	++	–	+	+	+	++	++	++
	Sericite	++	++	+	+	++	+	+	++	++	+	–	+
	Fluorite	+	+	+	+	+	–	+	+	–	+	+	+
	Zircon	+	+	–	+	+	–	+	+	+	+	+	++
	Thorite	–	+	+		+	–	–	+	–	–	–	–
	Xenotime	–	–	–	–	+	–	–	–	–	+	+	+
	Varvicite	+	+	+	+	+	+	–	+	+	+	+	+
	Ilmenite	+	–	–	–	+	–	+	+	–	+	+	+
	Magnetite	–	+	+	+	–	+	+	–	+	+	+	+
	Limonite	–	–	+	–	+	+	+	+	+	+	+	+
	Amblygonite	–	+	–	–	+	–	–	–	–	–	–	–

Note: RZ, IZ and CZ corresponds to the rim, intermidiate and core zone, respectively. +, ++, +++ and - means trace, moderate, abundant content and not observed, respectively

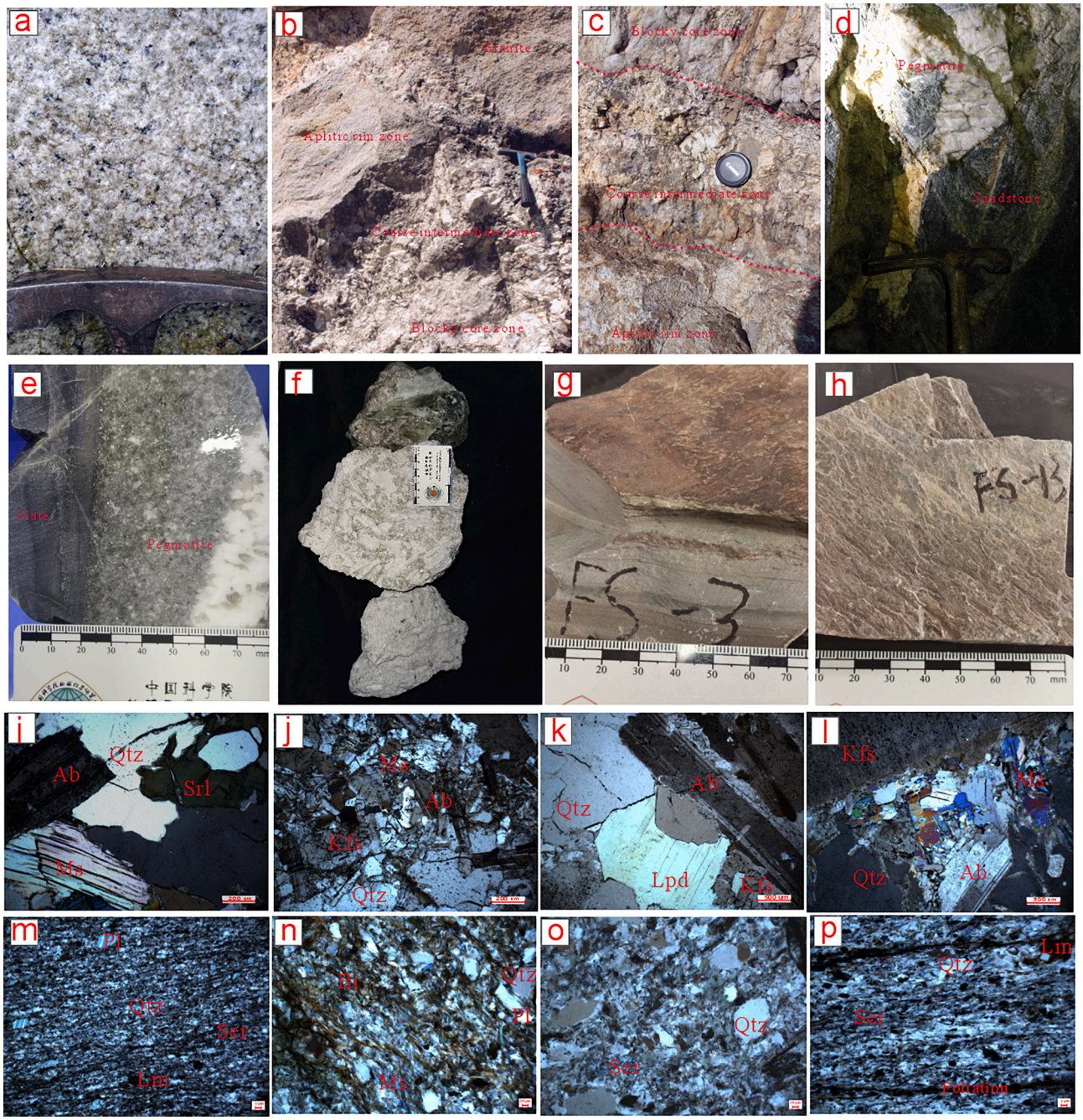

Fig. 3. Representative rock samples and contact relationships in the outcrop and under microscope, including the Fanjingshan granite in the outcrop (a) and under microscope (i), contact relationship between granite and pegmatite (b), among the internal zones of pegmatite (c), and between pegmatite and wall rocks (d and e), whole rock sample for single pegmatite (f) and microstructure (j-l), sedimentary rock samples shown as hand specimens (g and h) and micrographs (m-p). Abbreviation: Ab = albite, Bi = biotite, Kfs = k-feldspar, Lm = limonite, Lpd = lepidolite, Ms = muscovite, Pl = plagioclase, Qtz = quartz, and Ser = sericite.

branch vein has the weakest internal zoning and mineralization, and mainly consists of an aplitic rim zone (1–2 m thickness) and coarse intermediate zone (0.5–1 m thickness). Ore minerals mainly include columbite-Mn and a few cassiterite, with lower Nb, Ta and Sn abundances than 0.01% (BGGZP, 1962).

The No. 9 pegmatite is hosted by the slates of the Taojinhe Formation and mafic volcanic rocks with sharp contacts (Fig. 3d and e). As the largest pegmatite dyke, it consists of a main and several branch veins. The main vein exhibits a tabular shape with a length and thickness of about 1900 m and 0.2–7 m, respectively. The pegmatite has three internal zones, similar to those of the No. 7 pegmatite with gradual contact, and varying thicknesses. In the parts with constant thicknesses, the aplitic rim zone (thickness of 0.5–1 m), coarse intermediate zone (thickness of 1–2 m) and blocky core zone (thickness of 0.2–1 m) are continuously distributed from margin to the core. In the expansion parts, the zones are irregularly distributed, with increasing proportions of the intermediate and core zones and enhanced albitization, muscovitization and lepidolitization, and Li-Sn-Ta-Nb mineralization. Comparatively, the mineralization in the expansion parts is more intensive, which is featured by the increasing numbers of columbite-Mn and cassiterite ore minerals, especially Ta-rich minerals, such as microlite.

The No. 16 pegmatite shows a complex form and consists of two or three branch veins, a total length of 1400 m, and varying thicknesses from 0.5 to 5 m. The eastern extremity of the pegmatite connects with

the Taoshulin granite with a gradual contact (Fig. 3b), and the main body of the pegmatite is hosted by the slates and sandstones of the Taojinhe Formation (Fig. 3d and e). The No. 16 pegmatite has an aplitic rim zone, a coarse intermediate zone and a blocky core zone, with enhanced zoning at a distance from the Taoshulin granite. The aplitic zone occupies a large portion of the pegmatite; the coarse zone exhibits a discontinuous distribution along the rim zone, and the blocky core zone occurs only in the expansion part. Albitization and lepidolitization were locally developed in the intermediate zone with occurrence of CGMs, cassiterite and lepidolite. Combined with the mineral assemblages (Table 1), the Nos. 7, 9 and 16 pegmatites were classified as Li-P-B-Sn-Ta-Nb granitic pegmatite.

3. Sampling and analytical methods

Eight granite samples were collected from Mocaogou (FG-1 and FG-2), Zhangjiayan (FG-3 and FG-4) and Taoshulin (FG-5 to FG-8) granites, seven pegmatite samples were collected from the Nos. 16 (FP16-1 and FP16-2), 7 (FP7-1 and FP7-2) and 9 (FP9-1 to FP9-3) pegmatites, and thirteen sedimentary rock samples (FS-1 to FS-13) were collected from the Taojinhe Formation in the lower section of the Fanjingshan Group. To determine the compositions of the pegmatites, the pegmatite samples were proportionally collected from all the internal zones of the pegmatites (Fig. 3f), with the total quantity of each sample being approximately 10–15 kg. All samples were ground to a size so that they can be sifted through a sieve with 100 meshes per square inch. Next, 100 g of each sample was further ground and whole rock composition analysis was performed. The remaining samples were used for heavy mineral separation of the zircon grains.

Zircon U-Pb age and Lu-Hf isotopic composition analyses were conducted using laser ablation inductively coupled mass spectrometry (LA-ICP-MS) and laser ablation multi-collector inductively coupled mass spectrometry (LA-MCICP-MS) at the State Key Laboratory of Ore Deposit Geochemistry, Institute of Geochemistry, Chinese Academy of Sciences (SKLODG, IGCAS). The GeoLasPro 193 nm ArF laser-ablation system was combined with an Agilent 7700x ICP-MS system for U-Pb age analysis; the experimental conditions were a 30 μm spot diameter at a 10 Hz repetition rate, 30 s blank run of and 60 s ablation time. The selection and integration of the background and analytic signals, time drift correction, and quantitative calibration of trace element contents and U-Pb ages were conducted using ICPMSDataCal (Liu et al., 2008). Zircon 91,500 was used as an external standard; with the U-Th-Pb isotope ratios recommended by Wiedenbeck et al. (2004). Concordia diagrams and weighted mean ages were obtained by using Isoplot/Ex (ver. 3) (Ludwig, 2003). The uncertainties of the individual and weighted mean $^{206}Pb/^{238}U$ ages were reported at the 1σ and 2σ levels, respectively.

Zircon Lu-Hf isotope analyses were performed using a GeoLasPro 193 nm laser-ablation microprobe attached to a Nu Plasma MCICP-MS. The working conditions and data acquisition were similar to those described by Chen et al. (2019). A 40 μm spot size, 6 Hz repetition rate of and energy density of 6 $J{\cdot}cm^{-2}$ were used for all the analyses, and helium was used as the carrier gas. To evaluate the accuracy of the results and test the reliability of the correction protocols, two zircon standards of 91,500 and GJ-1 were regularly analyzed, with mean $^{176}Hf/^{177}Hf$ ratios of 0.282300 ± 0.000011 (2σ, n = 20) and 0.282009 ± 0.000009 (2σ, n = 20), respectively, which are consistent with the recommended values of 0.282307 ± 0.000058 and 0.282015 ± 0.000019 (Elhlou et al., 2006; Griffin et al., 2006), respectively.

Whole-rock chemical compositions were also determined at the SKLODG, IGCAS. The major elements were determined via X-ray fluorescence (XRF) on $LiBO_4$ fusion glass plates using an Axios PW4400 XRF spectrometer, and certified standards were used for calibration. The trace elements were measured via inductively coupled plasma mass spectrometry ICP-MS (PerkinElmer, ELAN DRC-e). The relative errors were <5% and the analytical errors for the major and trace elements were <1% and <10%, respectively.

The major compositions of the ore minerals were investigated using a JEOL JXA-8230 electron microprobe at the SKLODG, IGCAS. The operating condition includes were a 20 kV acceleration voltage, 20 nA beam current, 10 μm probe diameter, and counting times of 10 s and 5 s for element peak and background, respectively. The following standards were used for quantitative analyses: Ta metal (Ta, *Ma*), Nb metal (Nb, *La*), SnO_2 (Sn, *La*), almandine (Fe, *Ka*), $MnTiO_3$ (Mn and Ti, Ka), fluorapatite (Ca and F, *Ka*), albite (Na, *Ka*), W metal (W, *La*), uraninite (U and Th, *Ma*), and Sc (*Ka*, calculated off-line). All data were corrected using the ZAF routine.

4. Results

4.1. Petrography

Fanjingshan Granite. The granite is grey-white or light grey in the outcrop (Fig. 3a), has an equigranular texture in the hand specimen (Fig. 3a), and a microscopic picture (Fig. 3i). The rock-forming minerals primarily include 30%-40% quartz, 20%-30% K-feldspar, 20%-30% albite, 15%-25% muscovite, and 3%-5% schorl, with maximum grain sizes of 0.5 cm (Fig. 3i). The feldspar and muscovite minerals primarily exhibit subhedral-euhedral crystal habits, and the quartz exhibits anhedral-subhedral habits. Schorl generally exhibits an anhedral crystal habit with a spheroid shape. The accessory minerals mainly consist of apatite, garnet, and zircon, and the remaining accessory minerals are listed in Table 1.

Fanjingshan pegmatite. Each pegmatite sample consisted of three samples: one from each of the aplitic rim zone (RZ), coarse intermediate zone (IZ) and block core zone (CZ) (Fig. 3f). The samples from the RZ contained 30%-35% quartz, 20%-30% microcline, 15%-30% muscovite, 15%-30% albite, and 2%-3% schorl (Table 1) and are featured by fine grained minerals with grain sizes not exceeding 0.2 cm (Fig. 3j). The samples from the IZ contained 30%-45% quartz, 15%-25% microcline, 15%-20% muscovite, 20%-30% albite and 2%-3% schorl (Table 1) and are characterized by coarse grained minerals with sizes ranging from 0.5 to 5 cm (Fig. 3k and l). Microcline minerals from the RZ and IZ are commonly replaced by albite or muscovite. CGMs and cassiterite were commonly observed in these samples. The samples from the CZ varied in the rock-forming minerals contents and contained 50%-70% quartz, 20%-35% microcline, 3%-10% muscovite, 5%-15% albite and 3%-5% schorl (Table 1), with mineral grain sizes of 5–15 cm. The accessory minerals have uneven distributions in the different zones, and include apatite, spessartite, and so on (Table 1).

Sedimentary rocks from the Taojinhe Formation. Samples FS-1, FS-2, FS-3, FS-4, and FS-7 were collected from slates (Fig. 3g); they featureed cleavage development and contained 50%-55% clay minerals, 30%-35% quartz, 2%-10% plagioclase, 3%-5% chlorite, 3%-5% sericite, 2%-5% limonite, and 1%-3% calcite, with mineral grain sizes generally smaller than 5 μm (Fig. 3m). Samples FS-5, FS-6, FS-8, FS-9, and FS-12 were collected from siltstones and contained 45%-50% quartz, 10–20% sericite, 10%-20% muscovite, 5%-10% biotite and 3%-5% plagioclase, with mineral grain sizesgenerally smaller than 60 μm (Fig. 3n and o). Sample FS-10 was collected from calcareous sandstone and contained 55% quartz and 20% calcite, 15% lithic fragment 10% chlorite, and 5% sericite, with grain sizes<200 μm. Sample FS-13, collected from phyllite rock, was characterized by evident foliation and silky luster in the hand specimen (Fig. 3h), and crystalloblastic texture under a microscope (Fig. 3p); the sample mainly consisted of 50% clay minerals, 30% quartz, 15% sericite, and 5% limonite (Fig. 3p).

4.2. Whole rock major and trace compositions

Granite. FG-1 to FG-8 granite samples have high SiO_2 (71.85–79.61 wt%) and Al_2O_3 (11.70–16.09 wt%) contents; moderate Na_2O (2.97–4.68 wt%) and K_2O (2.79–4.10 wt%) contents; and low $Fe_2O_{3(T)}$ (0.81–1.18 wt%), CaO (0.18–0.51 wt%), P_2O_5, (0.16–0.38 wt%) and F

(0.1–0.3 wt%) contents; and MgO, MnO, and TiO_2 contents of <0.1 wt% (Supplementary table 3). According to the plot of SiO_2 vs. ($Na_2O + K_2O$), all the samples fall in the granite range in the total alkali-silica (TAS) diagram (Fig. 4a). They are strongly peraluminous with high Al_2O_3/($CaO + Na_2O + K_2O$) (A/CNK) andAl_2O_3/($Na_2O + K_2O$) (A/NK) molar ratios of 1.25–1.45 and 1.29–1.48, respectively (Fig. 4b, Supplementary Table 1), indicating an S-type granite. Except for K_2O, the CaO, Al_2O_3, MgO, P_2O_5, and Na_2O contents show negative correlations with SiO_2 in the Harker diagrams (Fig. 5a-e), and have low REE contents (5.11–34.19 ppm) with a negative Eu anomaly (Eu/Eu* = 0.02–0.05) and intense tetrad effect ($TE_{1,3}$ = 1.53–1.74) in the chondrite-normalized patterns (Fig. 6a, Supplementary Table 1). The samples show enrichment of the large ion lithophile elements (LILEs) of Rb and Pb and high field strength elements (HFSEs) of U, Ta, and Hf, the samples also exhibited depletion of Ba, Sr, Eu and light REEs in the primitive mantle-normalized trace element patterns (Fig. 6b).

Pegmatite. The samples of the Nos. 16 (FP16-1 and FP16-2), 9 (FP9-1 to FP9-3) and 7 (FP7-1 and FP7-2) pegmatites are composed of 71.53–80.87 wt% SiO_2, 11.84–17.57 wt% Al_2O_3, 2.83–6.93 wt% Na_2O, 0.51–6.07 wt% K_2O, 0.08–0.52 wt% $Fe_2O_{3(T)}$, 0.17–0.87 wt% CaO, 0.13–1.62 wt% P_2O_5, 0.1–0.2 wt% F, 0.02–0.24 wt% MgO, and 0.01–0.24 wt% MnO (Supplementary Table 1), similar to the granite samples mentioned above. The whole-rock samples of the pegmatites show silica and alkali contents similar to those of the granite samples (Fig. 4a), greater Al enrichmentl (Fig. 4b), and correlations similar to those of CaO, Al_2O_3, MgO, and P_2O_5 with SiO_2 (Fig. 5a-d). The K_2O and Na_2O contents show weak correlations with the SiO_2 content (Fig. 5e and f), which may be due to the non-uniform distributions of microcline, albite, and quartz in the pegmatites. The samples have extremely low REE contents (0.91–9.19 ppm), with varying Eu anomalies (Eu/Eu* = 0.07–4.90) and evident tetrad effects ($TE_{1,3}$ = 1.19–1.54) (Fig. 6a, Supplementary Table 1). The spider diagram also shows enrichment of Rb, Sr, U, Pb, Ta, and Hf and depletion of Ba and REEs (Fig. 6b).

Sedimentary rocks of the Taojinhe Formation. Samples FS-1 to FS-13, except for the sample FS-11 (due to strong weathering), were analyzed. They commonly have a higher SiO_2 (58.65–78.23 wt%) and lower Al_2O_3 (7.58–18.34 wt%) contents than those of post-Archean Australian average shale (PAAS) (Taylor and McLennan, 1985), and varying CaO (0.02–10.15 wt%), $Fe_2O_{3(T)}$ (1.00–10.70 wt%), K_2O (1.77–4.26 wt%), Na_2O (0.13–2.64 wt%), MgO (0.33–3.37 wt%), TiO_2 (0.57–0.84 wt%) and P_2O_5 (0.02–0.13 wt%) contents (Fig. 7a-e; Supplementary Table 2). The sedimentary rocks have moderate REE contents (134–239 ppm) and generally have flat REE patterns (La_N/Yb_N = 0.57–1.50) with no evident Ce and Eu anomalies (Ce/Ce* = 0.93–1.07 and Eu/Eu* = 0.79–1.04) in the upper continental crust (UCC)-normalized REE patterns (Fig. 8a; Supplementary Table 2). Samples FS-4 and FS-7, however, showed distinct patterns with relative enrichment of light REEs (La_N/Yb_N = 1.64) and negative Ce anomaly (Ce* = 0.47) for the former, and relative enrichment of heavy REEs (La_N/Yb_N = 0.45) for the latter (Supplementary Table 2). In the UCC-normalized spider diagram, most of the sedimentary rocks show subparallel HFSE patterns to that of the PAAS, with more enrichment of Rb (generally > 160 ppm) and depletion of Ba (mostly above 200 ppm) and Sr (7.93–156 ppm) than the latter. Additionally, sample FS-9 exhibited abnormal enrichments of Ta (14.5 ppm) and Nb (37.2 ppm) compared to the other samples and PAAS (Fig. 8b).

4.3. Major compositions of ore minerals

4.3.1. Columbite group minerals

The columbite group minerals (CGMs) are commonly observed in the Fanjingshan granite and pegmatite. In the samples from the Mocaogou (FG-2), Zhangjiayan (FG-3), and Taoshulin (FG-6) granite, the CGMs generally show schistose texture and the occurrence of anhedral aggregation (Fig. 9a) or euhedral monocrystals (Fig. 9b), with maximum grain size of 300 μm. They have homogeneous luminescence intensity in backscattered electron (BSE) images, and show intergrowth with albite and muscovite (Fig. 9a and b). In pegmatite, the CGMs from the No. 9 (FP-9) and No. 16 (FP-16) pegmatites generally show subhedral-anhedral tabular grains and homogeneous luminescence intensity in BSE images, with large grain sizes exceeding 1 mm (Fig. 9c and d). However, the CGMs from the No. 7 (FP-7) pegmatite show heterogeneous luminescence intensity, occurrences of euhedral monocrystals (Fig. 9e) or aggregation (Fig. 9f), intergrowth with cassiterite, microlite, and zircon, and relatively small grain sizes of 100–350 μm (Fig. 9e and f).

The results show that the CGMs from the granite samples have high Nb_2O_5 (45.622%–61.919%) and $FeO_{(T)}$ (10.121%–15.340%) contents, low Ta_2O_5 (13.013%–29.394%) and MnO (4.646%–9.036%) contents, relatively high WO_3 (2.926%–4.970%) and TiO_2 (1.651%-3.214%) contents, and relatively low Sc_2O_3 (mostly < 0.2%) and UO_2 (generally below the detection limit) contents. Comparatively, the CGMs from the pegmatite samples have increased Ta_2O_5 (14.380%-55.647%), MnO (16.223%–19.467%) and UO_2 (0.100%–1.624) contents, and decreased Nb_2O_5 (24.806%–60.390%), $FeO_{(T)}$ (0.097%–3.201%), WO_3 (0.284%–4.248%), TiO_2 (0.130%-2.484%) and Sc_2O_3 (mostly below detection limit) contents (Supplementary Table 3a). As shown in the compositional variation diagram (Fig. 10a), the CGMs show decreased non-formula elements from the granite to the pegmatite. In the Mn/(Mn +

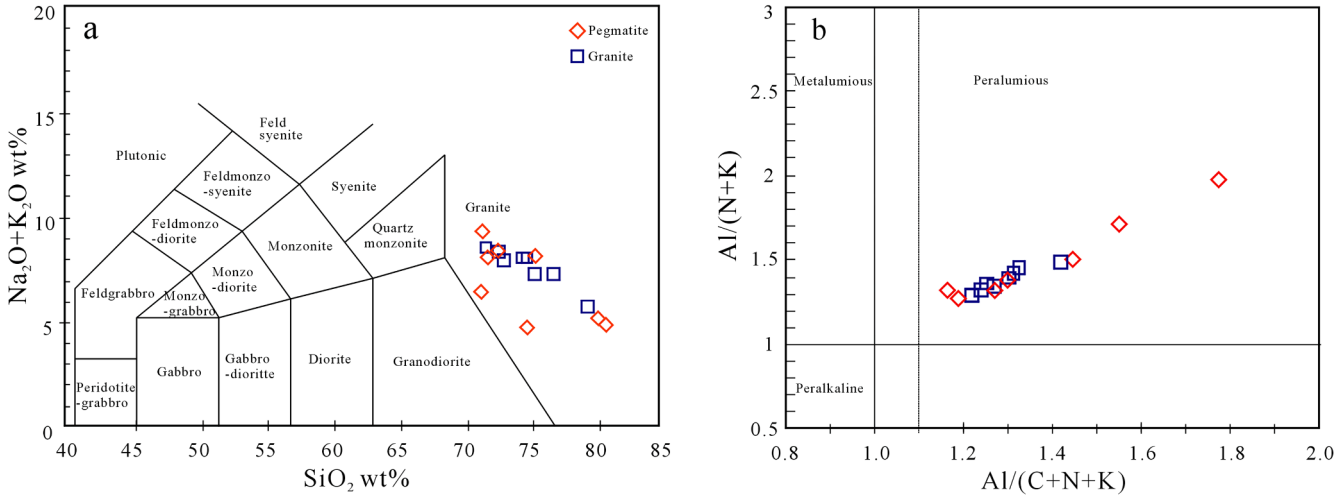

Fig. 4. Total alkali versus silica diagram (a, after (Gillespie and Styles, 1999)and Shand index plot (b, after (Shand, 1948)for the Fanjingshan granite and pegmatite samples. Where A/NK = molar (Al2O3/(Na2O + K2O)) and A/CNK = molar (Al2O3/(CaO + Na2O + K2O)).

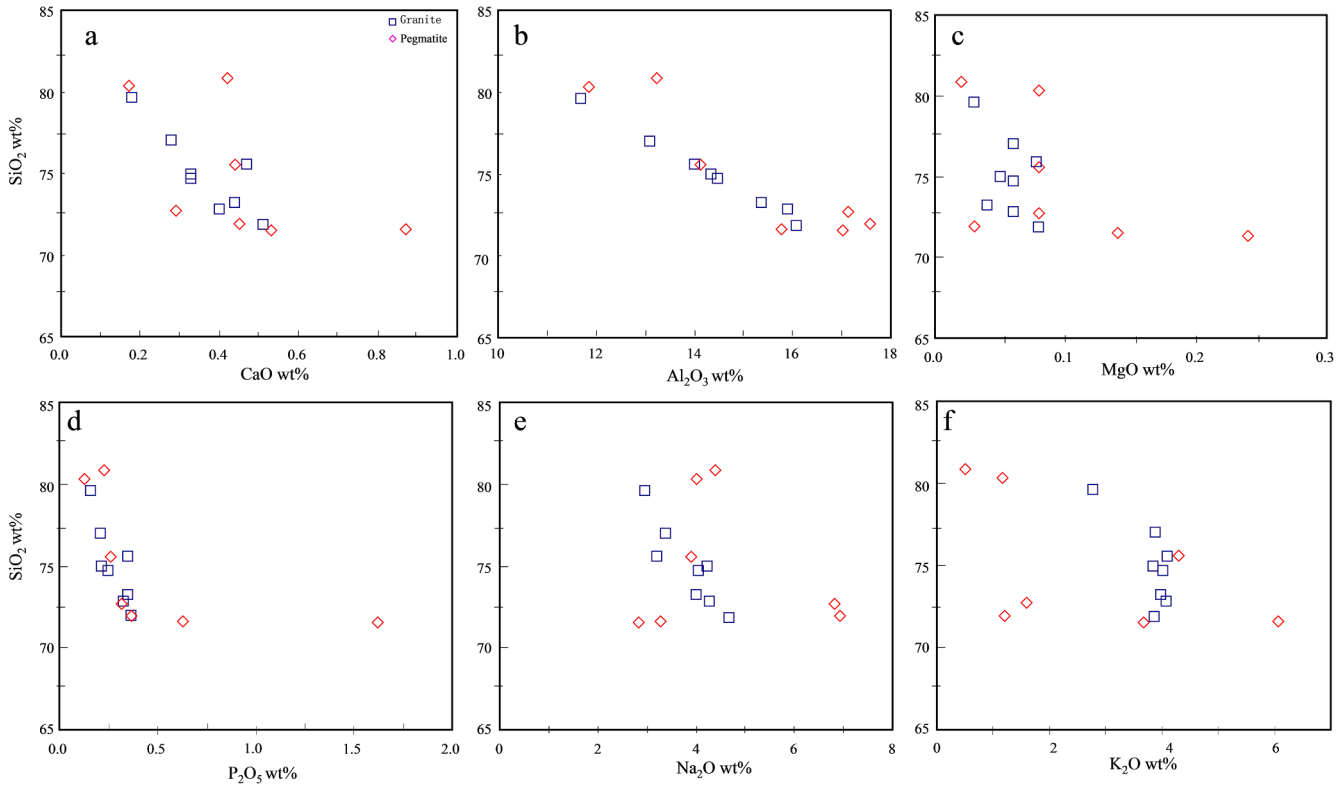

Fig. 5. Harker diagrams of CaO (a), Al_2O_3 (b), MgO (c), P_2O_5 (d), Na_2O (e) and K_2O (f) versus SiO_2 contents for the Fanjingshan granite and pegmatite samples.

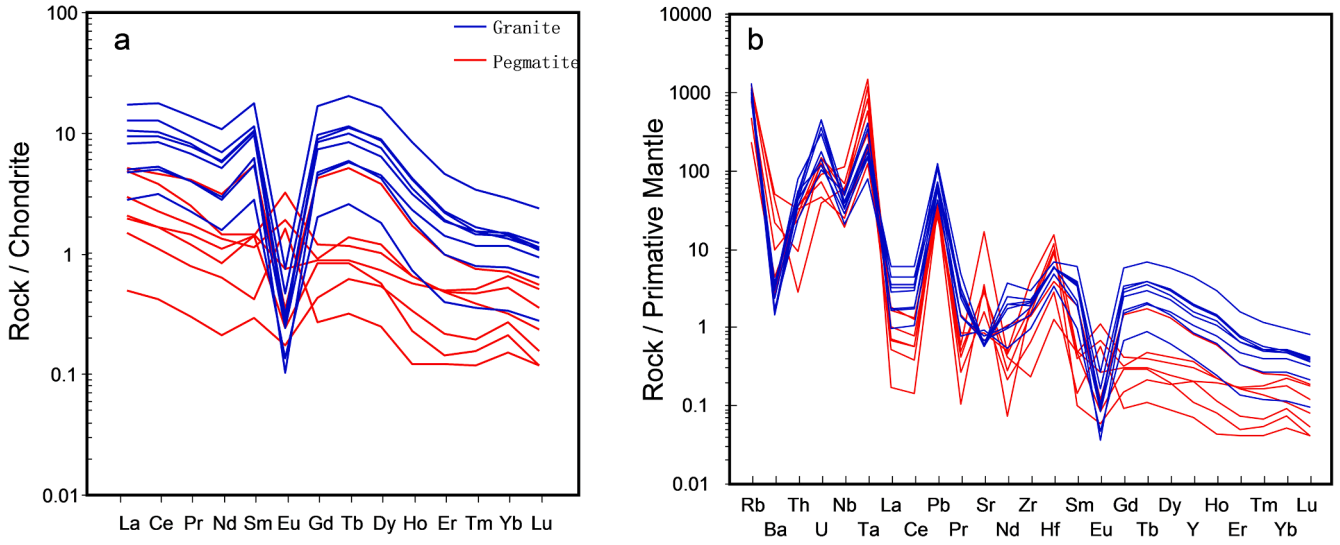

Fig. 6. Chondrite-normalized REE patterns (a) and primitive mantle normalized trace element spider patterns (b) of the Fanjingshan granite and pegmatite samples. Reference values of chondrite and primitive mantle are from Sun and McDonough (Sun and McDonough, 1989).

Fe) vs. Ta/(Ta + Nb) diagram (Fig. 10b), the CGMs from the granite and pegmatite fall into the columbite-Fe and columbite-Mn field, respectively, and a few grains from the No.7 pegmatite plot fall into the tantalite-Mn field.

4.3.2. Cassiterite

In addition to the CTGMs, cassiterite is the main ore mineral observed in the Fanjingshan granite and pegmatite. In granite samples FG-2 and FG-6, cassiterite is presented as subhedral monocrystal in albite, with homogeneous luminescence intensity in the BSE image and small grain sizes of 200–500 μm (Fig. 9g). In the pegmatite samples FP-7, FP-9 and FP-16, cassiterite exhibit similar morphological and optical features to those of FG-2 and FG-6 but with larger grain sizes >1 mm (Fig. 9h). The cassiterite grains from the granite samples have a high SnO_2 (98.181%-99.998%) content and low Nb_2O_5 (no>0.5%), Ta_2O_5 and WO_3 (all below the detection limit) contents. Comparatively, the cassiterite grains from the pegmatite samples have a lower SnO_2 (95.225%–99.173%) content and higher Nb_2O_5 (0.141%–1.119%) and WO_3 (0.122%–1.333%) contents. The cassiterites from the No. 7 pegmatite are especially rich in Ta, with Ta_2O_5 contents of 1.216%-2.880% (Supplementary Table 3b). A composition variation trend from the granite to the pegmatite is evident in the Fig. 10c.

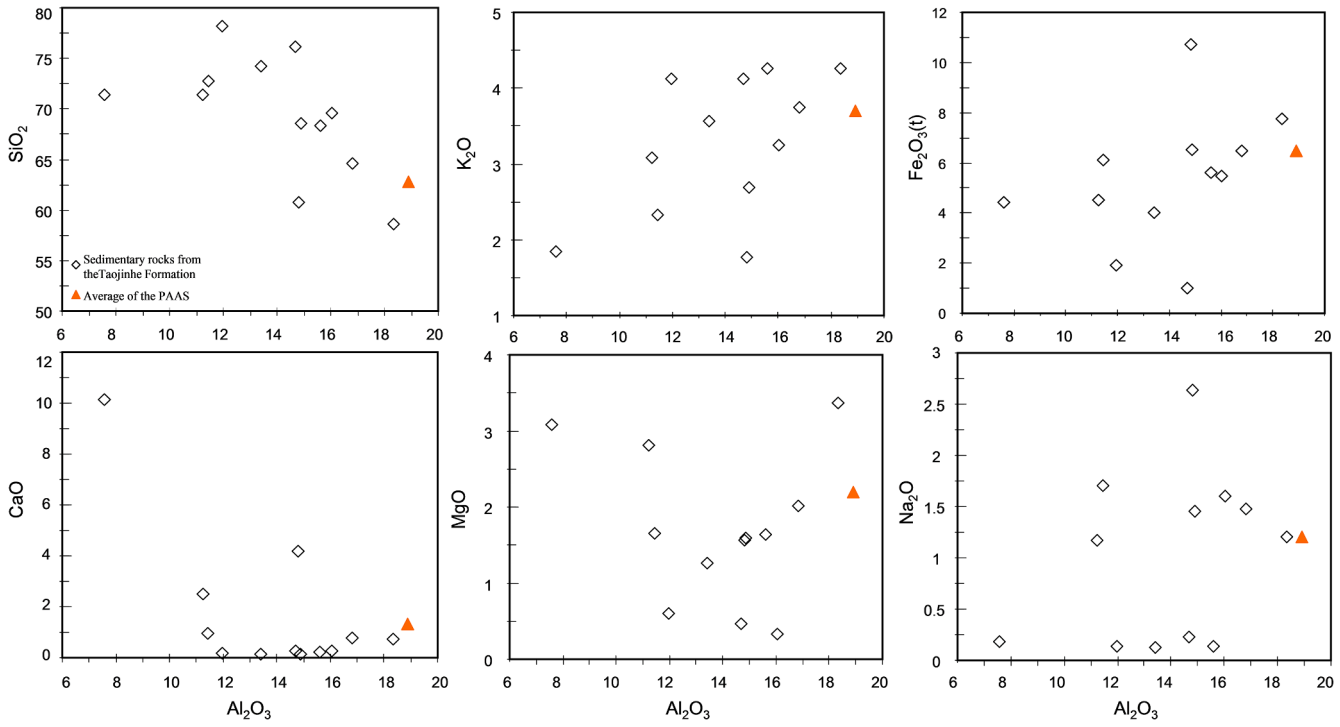

Fig. 7. Major composition diagrams for sedimentary rocks from the Taojinhe Formation of the lower Fanjingshan Group. Data of the average PAAS are from Taylor and McLennan (Taylor and McLennan, 1985).

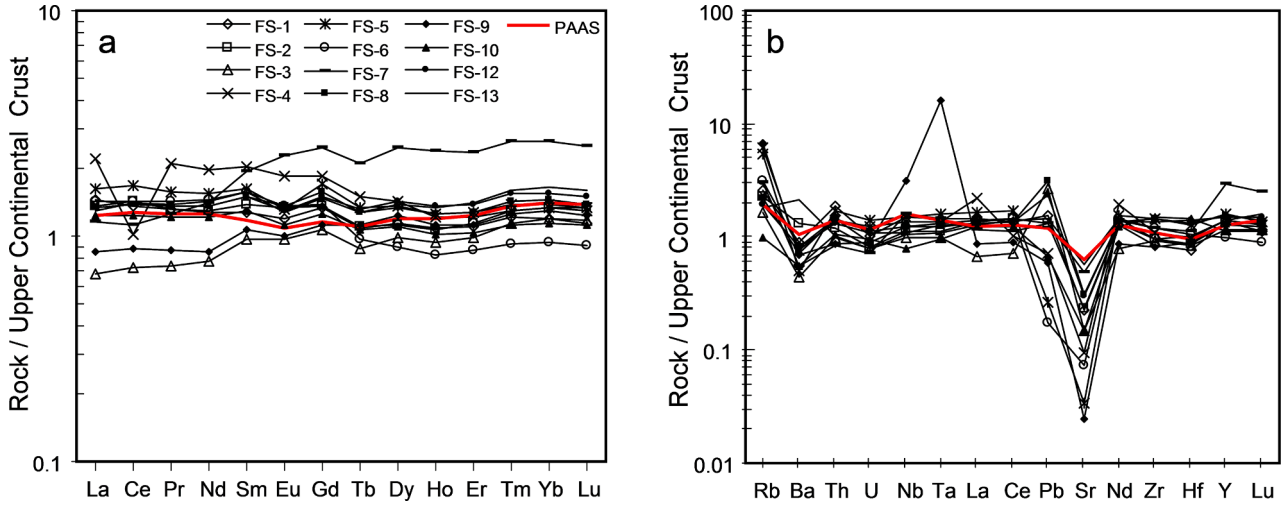

Fig. 8. Upper continental crust (UCC)-normalized REE patterns and spider diagrams of sedimentary rocks from Taojinhe Formation of the lower Fanjingshan Group. Reference values of UCC are from Taylor and McLennan (Taylor and McLennan, 1985).

4.3.3. *Microlite group minerals*

Compared to the CGMs and cassiterite, microlite group minerals are rare and observed only in the Nos.7 and 9 pegmatites. They are commonly small subhedral-anhedral grains (10–30 μm) and show intergrowth with CGMs, zircon and albite (Fig. 9f and i). The EPMA analysis results reveal that the microlite group minerals have high Ta_2O_5 (54.445%–77.658%) and low Nb_2O_5 (3.454%–15.042%) contents, and varying CaO (8.993%–14.607%) and Na_2O (2.106%–5.990%) contents (Supplementary Table 3c). Comparatively, the microlite grains from the No. 9 pegmatite have lower Ta_2O_5 and Na_2O and F contents, and higher Nb_2O_5, SnO_2, TiO_2, UO_2, MnO, and $FeO_{(T)}$ contents than those from the No. 7 pegmatite, as shown in the composition variation diagram (Fig. 10d).

4.4. *Zircon morphology, U-Pb ages and Hf isotopic compositions*

4.4.1. *Morphology*

The zircons in granite samples FG-1, FG-5 and FG-6 vary in size (90–120 μm) and commonly exhibit a faint yellow color and euhedral habit characterized by {100} + {101} crystal faces. In the cathode luminescence (CL) images, the zircons exhibit typical oscillatory zoning (Fig. 11a-c), and some zircons with an evident core-rim texture under CL (Spot 29 in Fig. 11a) were observed in these granite samples, indicating an inherited zircon occurrence. The zircons in pegmatite samples FP7-1, FP9-1 and FP16-1 vary in size (100–130 μm), are brown in color and are opaque with a euhedral habit characterized by {111} + {110} crystal faces. They commonly show weak luminescence with irregular (Spots 2, 3 and 6 in Fig. 11d), patchy (Spot 8 in Fig. 11e) and broadened

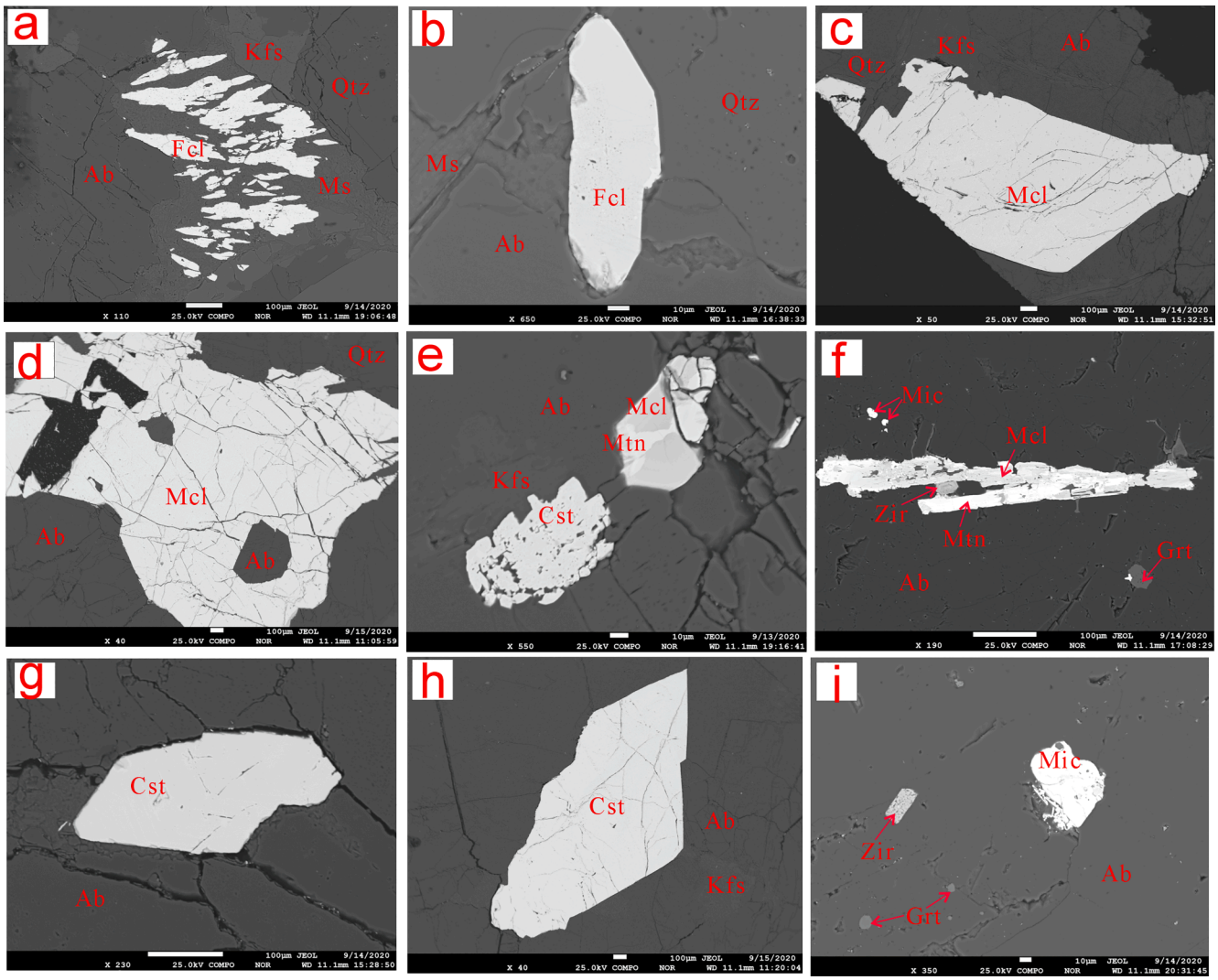

Fig. 9. Representative backscattered electron (BSE) images of rare metal minerals from the Fanjingshan granite and pegmatite. Ferrocolumbite in granite (a and b), mangancolumbite in pegmatite (c and d) and showing intergrowth with manganotantalite (e and f), cassiterite (e) and microlite (f), cassiterite in granite (g) and pegmatite (h), and microlite in pegmatite (i). Abbreviation: Ab = albite, Cst = cassiterite; Grt = garnet, Kfs = k-feldspar, Ms = muscovite, Mcl = mangancolumbite, Mic = microlite, Mtn = manganotantalite, Qtz = quartz, and Zir = zircon.

oscillatory zonings (Spots 2 and 6 in Fig. 11f) or no zoning under CL (Spots 1 and 10 in Fig. 11e).

4.4.2. U-Pb ages and Hf isotopic compositions of granite samples

Sample FG-1. A total of 31 zircon grains were identified, of which 19 have low Th and U contents of 45–552 ppm and 242–774 ppm, respectively, with Th/U ratios varying from 0.12 to 0.96. The 19 zircon grains define a $^{206}Pb/^{238}U$ age population range of 807 Ma–856 Ma (Supplementary Table 4) and a weighted mean $^{206}Pb/^{238}U$ age of 835.1 ± 9.9 Ma (Fig. 12a). The other 12 zircon grains with a core-rim texture have lower Th (62–305 ppm) and U (174–561 ppm) contents, and the inherited zircon cores yield concordant ages with $^{206}Pb/^{238}U$ ages varying from 1101 to 1839 Ma(Fig. 12a; Supplementary Table 4). Therefore, the mean age of 835.1 ± 9.9 Ma represents the granite formation time. 13 of the 19 zircon grains yield $^{176}Hf/^{177}Hf$ values ranging from 0.282021 to 0.282308. According to the $^{206}Pb/^{238}U$ ages of the 13 zircon grains, the calculated $\varepsilon_{Hf}(t)$ values range from + 1.13 to −8.63 with T_{DM2} model ages of 1650–2258 Ma (Supplementary Table 5).

Sample FG-3. The 26 dated zircons have Th and U contents in the ranges of 45–680 ppm and 137–1147 ppm, respectively, with Th/U ratios of 0.09–0.99. They have $^{206}Pb/^{238}U$ ages of 802–851 Ma (Supplementary Table 4) with a weighted mean $^{206}Pb/^{238}U$ age of 834.5 ± 8.4 Ma (Fig. 12b). 13 zircons yield $^{176}Hf/^{177}Hf$ values ranging from 0.282053 to 0.282220. According to the $^{206}Pb/^{238}U$ ages of 814–851 Ma, the calculated $\varepsilon_{Hf}(t)$ values range from −1.41 to −7.42 with T_{DM2} model ages of 1808–2182 Ma (Supplementary Table 5).

Sample FG-6. The 23 dated zircons have Th and U contents in the ranges of 48–554 ppm and 208–1410 ppm, respectively, Th/U ratios ranging from 0.05 to 0.72, $^{206}Pb/^{238}U$ ages of 818–845 Ma (Supplementary Table 4) and a weighted mean $^{206}Pb/^{238}U$ age of 830.0 ± 8.7 Ma (Fig. 12c). 13 zircon grains yield $^{176}Hf/^{177}Hf$ values ranging from 0.282046 to 0.282207 and according to their $^{206}Pb/^{238}U$ ages, the calculated $\varepsilon_{Hf}(t)$ values range from −2.03 to −7.91 with T_{DM2} model ages of 1844–2210 Ma (Supplementary Table 5).

4.4.3. U-Pb age and Hf isotopic composition of pegmatite sample

Sample FP16-1. The dated 16 zircon grains have Th and U contents in the ranges of 75–3879 ppm and 178–2209 ppm, respectively, with high Th/U ratios of 0.41–1.76. They defined a $^{206}Pb/^{238}U$ age population range of 823–836 Ma (Supplementary Table 4) and a weighted mean $^{206}Pb/^{238}U$ age of 832.0 ± 9.1 Ma (Fig. 12f) which is regarded as the pegmatite formation age. 13 zircon grains yield $^{176}Hf/^{177}Hf$ values ranging from 0.281990 to 0.282206. According to their $^{206}Pb/^{238}U$ ages of 829–836 Ma, the calculated $\varepsilon_{Hf}(t)$ values range from −1.82 to −9.51

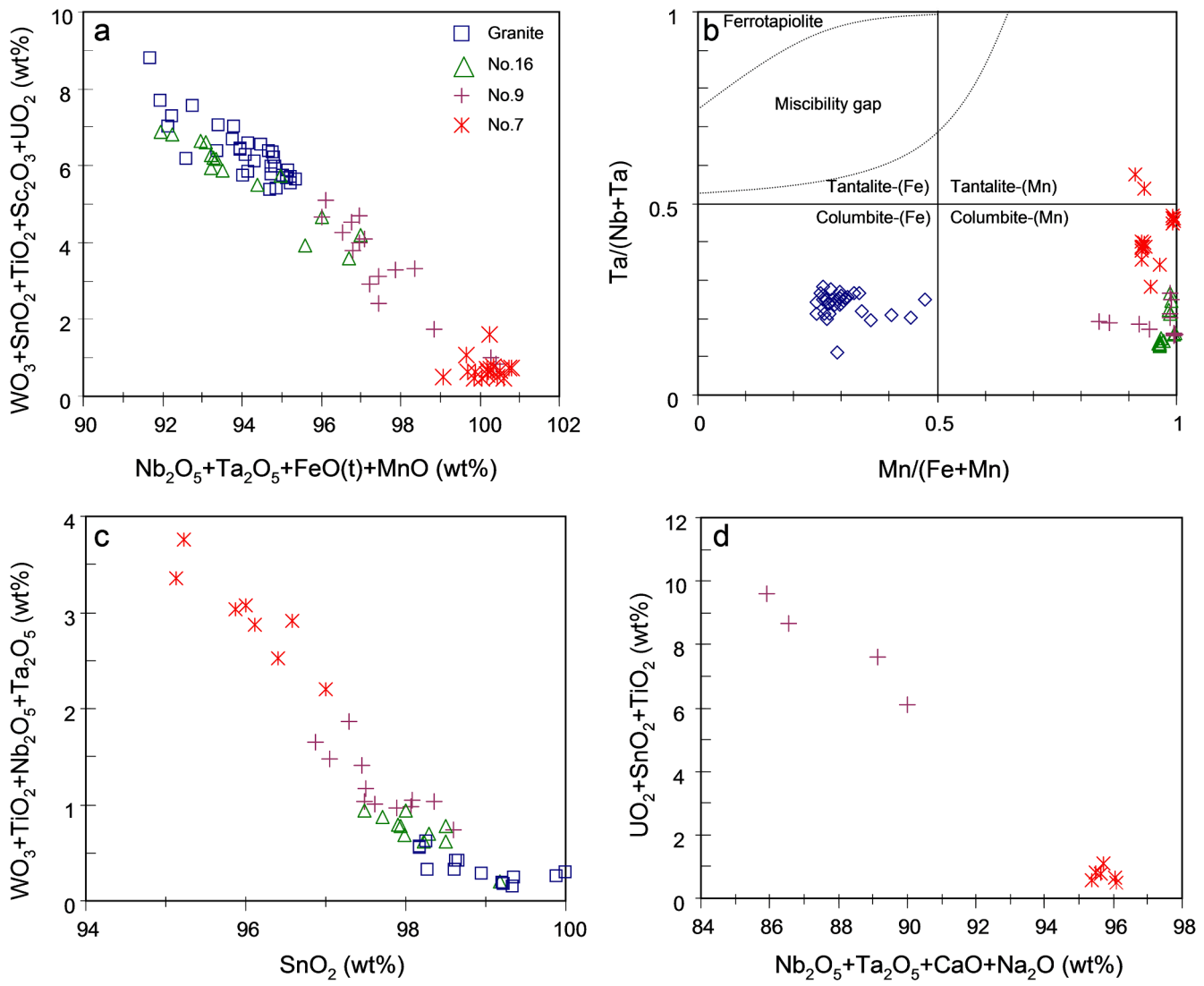

Fig. 10. Composition variation diagrams of rare metal minerals from the Fanjingshan granite and pegmatite. Columbite group minerals (a) and their Mn/(Fe + Mn) vs. Ta/(Nb + Ta) quadrilateral diagram (b), cassiterite (c) and mircrolite (d).

with T_{DM2} model ages of 1832–2310 Ma (Supplementary Table 5).

Sample FP9-1. The 23 dated zircons have Th and U contents varying from 57 to 359 ppm and 202 to 2233 ppm, respectively, Th/U ratios of 0.08–0.61, $^{206}Pb/^{238}U$ ages of 802–846 Ma (Supplementary Table 4) with a weighted mean $^{206}Pb/^{238}U$ age of 829.8 ± 8.7 Ma (Fig. 12e). 13 zircons yield $^{176}Hf/^{177}Hf$ values ranging from 0.282009 to 0.282216. According to their $^{206}Pb/^{238}U$ ages of 802–846 Ma, the calculated $\varepsilon_{Hf}(t)$ values range from −1.87 to −8.98 with T_{DM2} model ages of 1833–2275 Ma (Supplementary Table 5).

Sample FP7-1. The 16 dated zircon grains have Th and U contents ion the ranges of 77–1414 ppm and 225–2722 ppm, respectively, with corresponding Th/U ratios of 0.13–0.68. They defined a $^{206}Pb/^{238}U$ age population range of 812 Ma–838 Ma (Supplementary Table 4) and a weighted mean $^{206}Pb/^{238}U$ age of 827.0 ± 11 Ma (Fig. 12f) which is regarded as the pegmatite formation age. 13 zircon grains yield $^{176}Hf/^{177}Hf$ values ranging from 0.282007 to 0.282206. According to their $^{206}Pb/^{238}U$ ages of 812–838 Ma, the calculated $\varepsilon_{Hf}(t)$ values range from −1.97 to −9.35 with T_{DM2} model ages of 1838–2296 Ma (Supplementary Table 5).

5. Discussion

5.1. Relationship between the Fanjingshan granite and pegmatite

5.1.1. Temporal-spatial relationships

According to the classical model, pegmatites derived from granitic melts are commonly distributed in or around their parental granites, and show increasing fractionation degrees with increasing spatial distance from their parental rocks (e.g., Trueman and Černý, 1982; Černý, 1991; Hulsbosch et al., 2014). Three main mechanisms for the segregation of pegmatite derivatives have been proposed which include (1) filter pressing, fluid transport, and/or gravitational convection–diffusion, (2) crystal-melt fractionation, and (3) buoyant rise of local segregation (e.g., Černý and Meintzer, 1988; Černý, 1991). The Li-, Cs-, and Ta-rich pegmatites commonly show certain regional zonation in the peripheral area of their S-type parental granites (e.g., Trueman and Černý, 1982; Černý, 1991) with a maxima distance of 10 km (Selway et al., 2005), indicating the segregation of pegmatites dominated by filter pressing and fluid transport. Comparatively, segregation of the Nb-, Y-, and F-rich pegmatites from their source rock is difficult due to their relatively dry and viscous compositions,they are therefore restricted in or very close to their parental A-type granites without regional zonation, indicating the dominant segregation of crystal-melt fractionation (Černý, 1991).

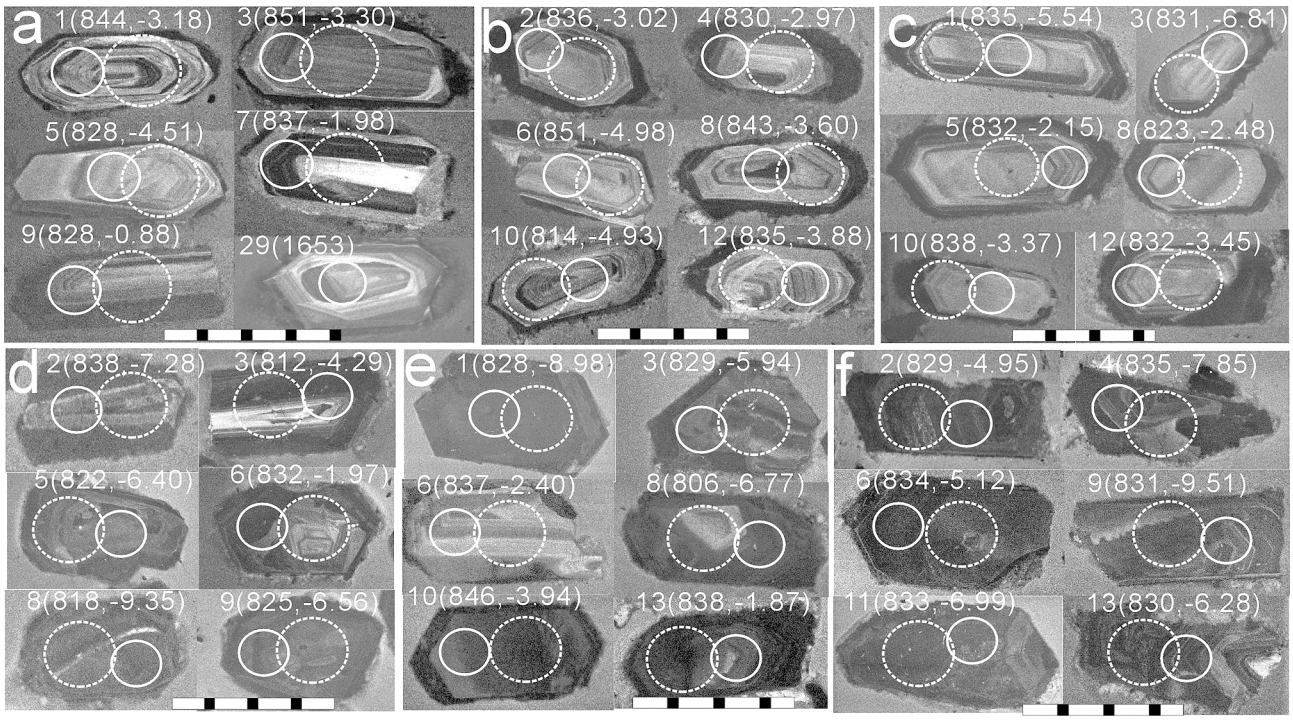

Fig. 11. Representative cathodoluminescence (CL) images of zircon, showing the laser analytic spots with $^{206}Pb/^{238}U$ ages and/or εHf(t) values. (a), (b), (c), (d), (e) and (f) show zircons from the samples of FG-1, FG-3, FG-6, FP16-1, FP9-1 and FP7-1, respectively. Scale bars correspond to 100 μm.

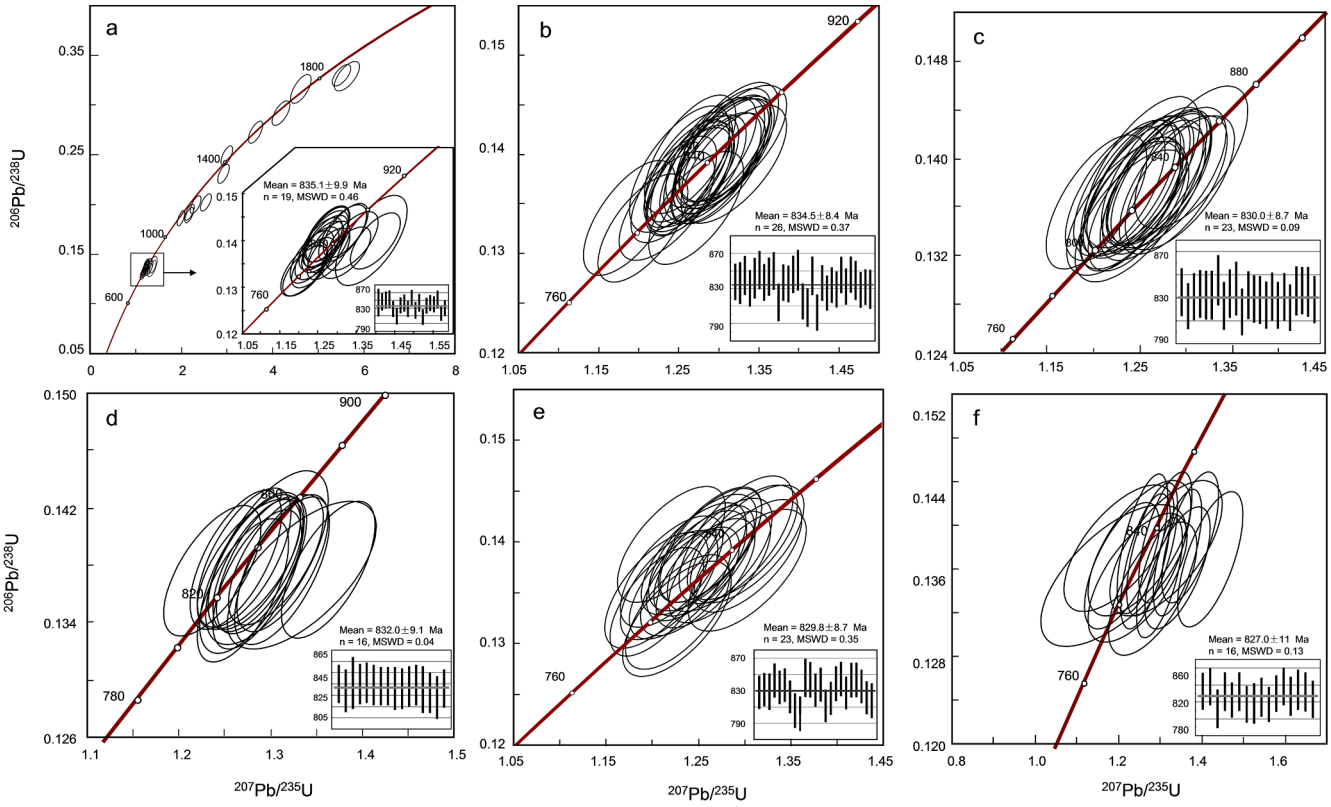

Fig. 12. Concordia diagrams with weighted mean ages of zircons from the samples of FG-1(a), FG-3(b), FG-6(c), FP16-1(d), FP9-1(e) and FP7-1(f), respectively. Only the inherited zircons in the FG-1 sample were analyzed (a). Error ovals are 1 sigma and mean ages given as 2 sigma.

Therefore, the relationship between the specified granite and neighboring pegmatites can be roughly evaluated through detailed geological surveys.

It is difficult to distinguish and delineate regional zonation for the pegmatites in the Fanjingshan area, due to the limited numbers and distribution ranges. However, the Fanjingshan granite and neighboring

pegmatites show emplacement control from the Zhangjiayan anticline and the Taojinhe Formation of the Fanjingshan Group and were intersected by the Taojinhe Fault, indicating the identical tectonic-dynamic settings and spatial connections between the Fanjingshan granite and pegmatite. The pegmatites are located within 200 m of the Taoshulin and Mocaogou granites (Fig. 2), and the No. 16 pegmatite shows a physical link to the Taoshulin granite with gradual contact between them (Fig. 3b). In addition, the increasing mineralization grade, the enhanced internal zoning and the decreasing proportion of aplitic wall zone from the No. 16 to No. 7 pegmatite indicate the enhanced fractionation degree and the temperature gap between pegmatite-forming melts and wall rocks with increasing distance from the source granite (London, 2008, 2014). In addition to the spatial relation, the temporal connection between the Fanjingshan granite and neighboring pegmatites was verified by zircon U-Pb dating. As mentioned above, the three samples collected from Mocaogou (FG-1), Zhangjiayan (FG-3) and Taoshulin (FG-6) granites in the Fanjingshan area have zircon U-Pb ages of 835.1 ± 9.9 Ma, 834.5 ± 8.4 Ma and 830.0 ± 8.7 Ma (Fig. 12a-c), respectively, and the Nos. 16 (FP16-1), 9 (FP9-1) and 7 (FP7-1) pegmatites have zircon U-Pb ages of 832.0 ± 9.1 Ma, 829.8 ± 8.7 Ma and 827.0 ± 11 Ma (Fig. 12d-f), respectively. The ages of the three granites are consistent with previous dating results of 827–835 Ma (Wang et al., 2011; Zhao et al., 2011) . The pegmatite ages are slightly late to or consistent with those of the granites, indicating that they were synchronously formed during Neoproterozoic. Therefore, the temporal-spatial connections between the Fanjingshan granite and surrounding pegmatites suggest a genetic relationship between them.

5.1.2. Source-differentiation relationships

It is no doubt that the pegmatite derivatives and their parental rocks have a common source. Although the pegmatite-forming melts could be contaminated by wall rocks during mobilization and after emplacement, the original melt compositions are not significantly modified by the wall rock due to the low temperature of the melts (commonly below 700 ℃) (London, 2008; Černý et al., 2012a). One typical contamination example is skarn occurrence in contact zones, which results from the intense contact metamorphism between the pegmatite-forming melt and Ca-rich wall rock after emplacement (Dill, 2016). However, skarn formation screens most of the heterogeneous materials from wall rocks, which helps retain the primary component of the pegmatite-forming melt. The pegmatites that are altered or reworked after solidification (named as pseudopegmatite according to Dill (2015b)) can also preserve the pristine isotope information of the source, especially for the zircon Hf isotope due to the robust stability of zircon and high blocking temperature of the Lu-Hf isotope system (e.g., Kinny and Maas, 2003). Additionally, a previous work has demonstrated that the igneous and hydrothermal zircons formed during the magmatic and hydrothermal stages of pegmatite-forming melt evolution, respectively, maintain the same Hf isotope compositions (Lv et al., 2012), indicating the limited effect of fluid exsolution and alteration on Lu-Hf isotope fractionation. Consequently, a zircon Hf isotope study was utilized to determine the relationship between the Fanjingshan granite and neighboring pegmatites, which reported that the zircons from the Mocaogou (FG-1), Zhangjiayan (FG-3), and Taoshulin (FG-6) granites mostly have negative $\varepsilon_{Hf}(t)$ values ranging from +1.13 to −8.63 (only one positive value), with corresponding T_{DM2} model ages of 1650–2258 Ma. The zircons from the Nos. 16 (FP16-1), 9 (FP9-1), and 7 (FP7-1) pegmatites have $\varepsilon_{Hf}(t)$ values range from −1.82 to −9.51, with T_{DM2} model ages of 1832–2310 Ma (Supplementary Table 5). Therefore, the zircon Hf isotope study demonstrates that the studied pegmatites have consistent isotope compositions with the Fanjingshan granite, indicating a common source. The overall enriched Hf isotopic compositions and older model ages (1650–2310 Ma) suggest that the source of the Fanjingshan granite and pegmatite may originate from the Paleoproterozoic crust (Fig. 13).

Although the temporal-spatial and source connections support the genetic relationship between the Fanjingshan granite and pegmatite, their degrees of differentiation should also be determined to verify a 'brotherhood' or 'mother-child' relationship. The Fanjingshan granite and pegmatite both have high SiO_2 and Al_2O_3 contents, moderate K_2O +

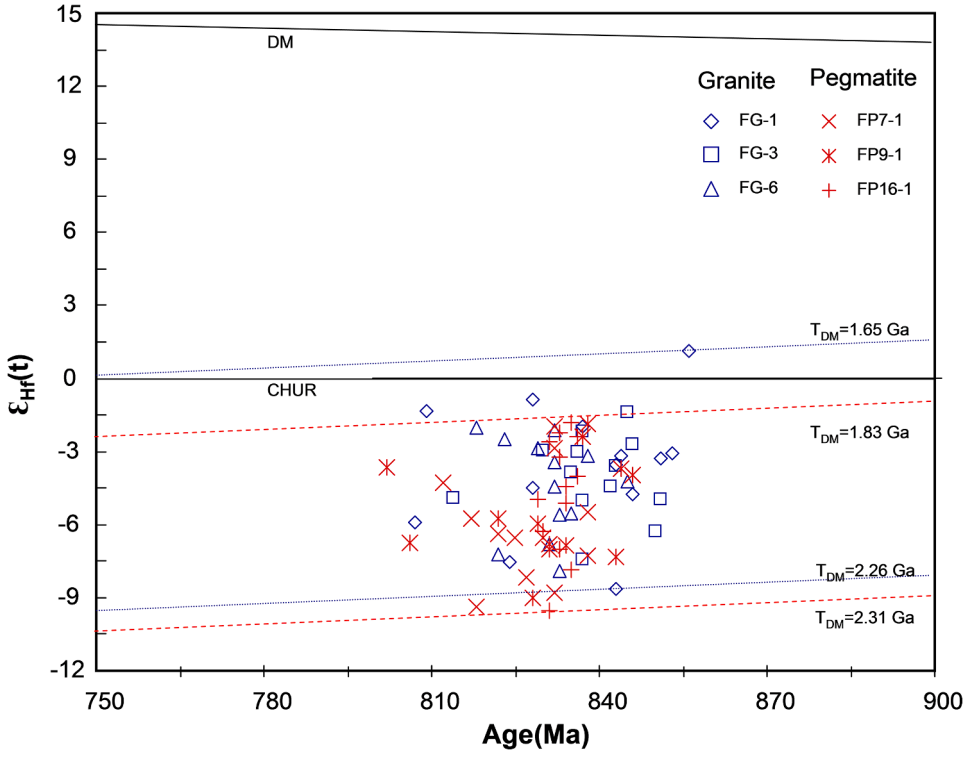

Fig. 13. Diagram of $\varepsilon_{Hf}(t)$ value versus crystallization age of zircons from the Fanjingshan granite and pegmatite. DM and CHUR are abbreviations of depleted mantle and chondrite uniform reservoir.

Na_2O alkali, and low CaO, $Fe_2O_{3(T)}$ and MgO contents (Supplementary Table 1). The pegmatites show larger variations in the major components, particularly for K_2O and Na_2O (Fig. 5e and f), indicating the nonuniform distributions of microcline and albite in the internal zones of pegmatites. The similar major compositions of the granite and pegmatite reflect the eutectic components after a high degree of differentiation. Previous studies have noted that trace elements show greater variations than major elements during the successive evolution of the fertile granites (e.g., Černý, 1991). Analogously, the differentiation trend from the Mocaogou, Zhangjiayan and Taoshulin granites to the Nos. 16, 9 and 7 pegmatites is difficult to distinguish by their major components (Fig. 5; however, the differentiation is evident in the REEs and rare metal elements (RMEs). The granites and pegmatites show similar REE patterns with an evident "tetrad effect" (Fig. 6a), indicating a high degree of differentiation and intense melt-fluid interaction (Irber, 1999). A recent study suggested that the lanthanide tetrad feature in rocks and minerals is associated with the water–rock interactions during surface weathering and the chemical properties of the coexisting fluid, especially the redox and pH conditions (Abedini et al., 2018). We don't think that the tetrad effects in the Fanjingshan granite and pegmatite were caused by water–rock interactions during surface weathering as suggested by Abedini et al. (2018); but we agree that the role and chemical property of aqueous fluid are critical for the tetrad effect formation during differentiation of granitic melt. In addition, the REE contents significantly decrease from the granites (average value of 14.9 ppm) to the pegmatites (average value of 3.4 ppm), and the Li, Be, Sn, Nb, Ta and Hf contents increase from the granites (averages values of 223 ppm, 1.6 ppm, 44 ppm, 26 ppm, 8.8 ppm, and 1.7 ppm, respectively) to the pegmatites (606 ppm, 3.6 ppm, 55 ppm, 39 ppm, 27 ppm, and 2.4 ppm, respectively) (Supplementary Table 1). The Nb/Ta, Zr/Hf, K/Rb and Mg/Li ratios of the whole rock are effective indicators of the degree of differentiation of the granite-pegmatite suite (Selway et al., 2005; Černý et al., 2012a) and show decreasing trends from the granites (averages values of 3.3, 12.6, 50 and 2.6, respectively) to the pegmatites (averages values of 1.9, 7.9, 35 and 1.1, respectively) (Fig. 14; Supplementary Table 1).

In addition to the evidence mentioned above, similar mineralization in the Fanjingshan granite and pegmatite also supports the differentiation trend from the granite to pegmatite. First, they both have Sn-Ta-Nb mineralization featured by the pervasive occurrence of cassiterite and CGMs (Fig. 9). The composition transition of the CGMs from the columbite-Fe in granite to the columbite-Mn and tantalite-Mn in pegmatite (Fig. 10a and b) indicates the melt differentiation and Fe, Mn, Nb, and Ta fractionation of in the system. The transformation of Nb- and Ta-rich minerals from the CGMs to the microlite group in pegmatite (Fig. 9) and the increasing Ta abundance in cassiterite from granite to pegmatite (Fig. 10c) indicate additional Ta enrichment during the differentiation of melt. Therefore, the REE and RME variations, Nb/Ta, Zr/Hf, K/Rb, and Mg/Li ratios and ore mineral compositions indicate a differentiation trend from the Fanjingshan granite to the surrounding pegmatites.

In conclusion, the Nos. 16, 9 and 7 rare metal pegmatites belong to the Li-P-B-Sn-Ta-Nb granitic pegmatite in the CMS classification (e.g., Dill, 2015a, 2015b, 2016). They are derivatives of the Fanjingshan S-type granite in the western JO, according to their temporal-spatial and source-differentiation connections. The Fanjingshan pegmatite is the only confirmed Neoproterozoic rare metal pegmatite in the JO till date.

5.2. *Provenance of the Taojinhe Formation and its implications*

The deposition time of the Fanjingshan Group has been confined by the zircon chronology of the sedimentary and volcanic rocks in the group, with age range of ca. 870–820 Ma (e.g., Zhou et al., 2009; Wang et al., 2014) . The Fanjingshan granite-pegmatite suite has a formation age of ca. 830 Ma as mentioned above, indicating a synsedimentary magma event in the southwestern JO. The Fanjingshan granite-pegmatite suite intruded in the Taojinhe Formation, the lowest section of the Fanjinghsan Group, implying that the Taojinhe Formation could be the source of the suite. Therefore, a geochemical study of the Taojinhe Formation could provide information regarding the source or tectonic setting of the granite-pegmatite suite.

5.2.1. *Provenance of the Taojinhe Formation*

The sedimentary rocks in the Taojinhe Formation have Chemical Index of Alteration (CIA) values of 58–77 (Supplementary Table 4), with an average of 70, which is similar to the PAAS value (69; Taylor and McLennan, 1985) (Fig. 13a). High CIA values (>75) generally reflect the removal of labile cations (e.g., Ca^{2+}, Na^{+}, and K^{+}) relative to stable residual components (Al^{3+} and Ti^{4+}) from the source during weathering process (e.g., Nesbitt and Young, 1984). This reflects a relatively strong chemical weathering of the source or the presence of compositionally mature Al-rich minerals produced by weathering (e.g., Gao et al., 1999; Joo et al., 2005). The varying CIA values of the studied sedimentary rocks indicate that the source of the Taojinhe Formation contains both weak and intense weathered materials. In addition, the sedimentary rocks in the Taojinhe Formation have varying Index of Compositional Variability (ICV) values of 0.53–4.25 (Supplementary Table 2), with an average of 1.35 (1.08 without considering the 4.25 value of sample FS-10), which is higher than that of PAAS (ICV = 0.85, (Taylor and McLennan, 1985) (Fig. 15a). High ICV values (>1) reflect low clay

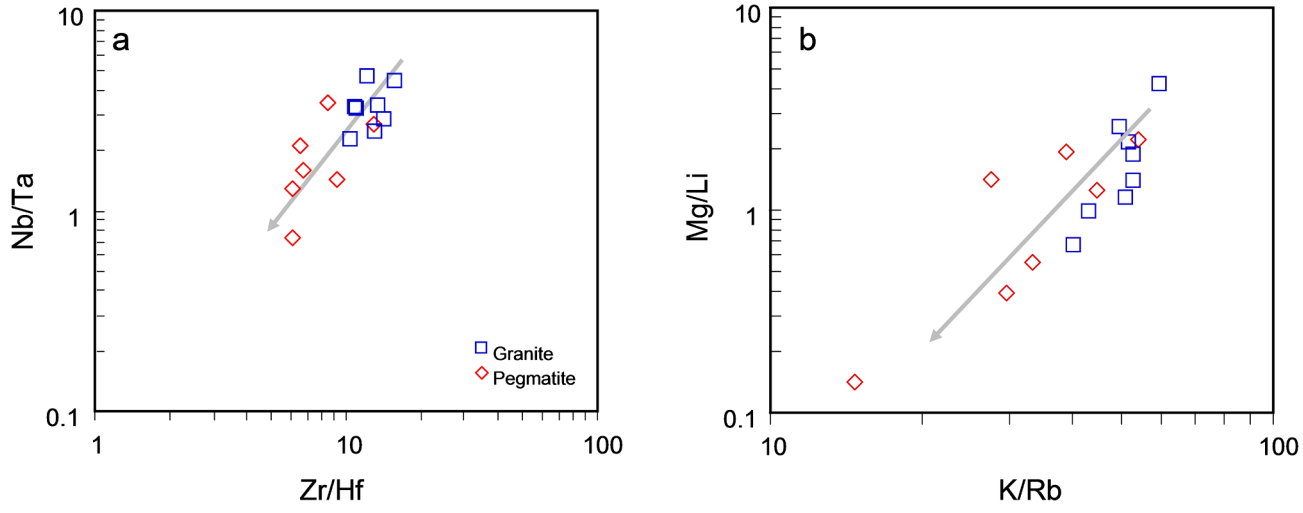

Fig. 14. Zr/Hf versus Nb/Ta (a) and K/Rb versus Mg/Li (b) diagrams for the differentiation of the Fanjingshan granite and pegmatite.

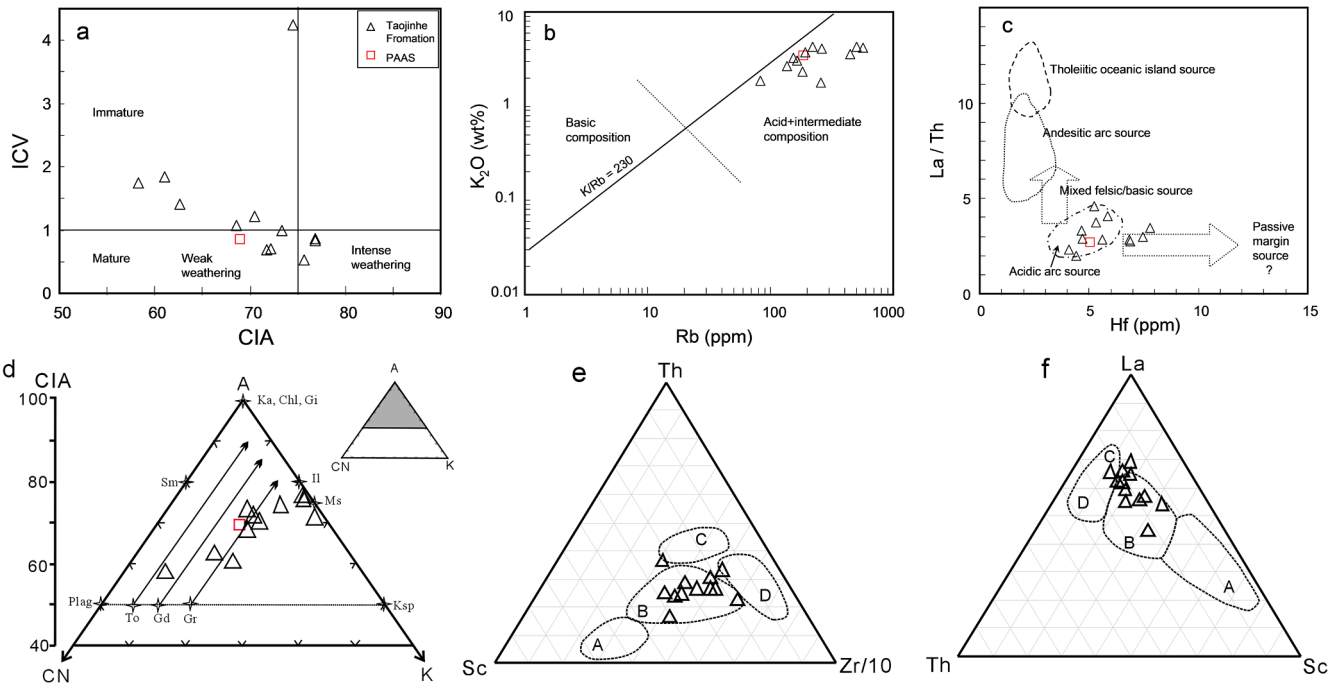

Fig. 15. Composition, source and deposition setting discrimination diagrams for the Taojinhe Formation of the lower Fanjingshan Group, including Chemical Index of Alteration (CIA) versus Index of Compositional Variability (ICV) diagram (a) after Cox et al. (1995); K_2O versus Rb diagram (b) after Floyd et al. (1989); La/Th versus Hf diagram (c) after Floyd and Leveridge (1987); ACNK ternary diagram (d) after (Fedo et al., 1995) (CIA values range from 50 for fresh primary igneous rocks to a maximum of 100 for the most weathered rocks, and data for tonalite (To), granodiorite (Gd) and granite (Gr) are from (Condie, 1993)), Th-Sc-Zr/10 (e) and La-Th-Sc (f) ternary diagrams after Roser and Korsch (1986) and Bhatia and Crook (1986).

minerals and high K_2O, Na_2O and CaO contents (e.g., Cox et al., 1995), indicating immature sources or first-cycle deposits in an active margin setting (e.g., Van de Kamp and Leake, 1985). Therefore, the varying ICV values reflect a mixture of immature and mature sources for the Taojinhe Formation.

K and Rb are commonly enriched in acidic-intermediate igneous rocks and are sensitive to sedimentary recycling; therefore, the Rb abundance and K/Rb ratio of sedimentary rocks can effectively reflect the source composition (e.g., Shaw, 1968; Floyd et al., 1989). The sedimentary rocks in the Taojinhe Formation have high Rb concentrations of 82–507 ppm (Supplementary Table 2) and lower K/Rb ratios (57–176) than that of the average value of crust (230, (Shaw, 1968) (Fig. 15b), indicating an acidic igneous source. In addition, the sedimentary rocks have low La/Th ratios (2.3–4.6) and moderate Hf concentrations (4.06–7.78 ppm) (Supplementary Table 2), and mostly fall in the range of acidic arc source (Fig. 15c). Moreover, most of the sedimentary rock samples plot in the granite trend, and a few samples with high CIA values deviate slightly from this trend and are close to the scope between illite and muscovite in the ACNK diagram (Fig. 15d), implying that the sedimentary rocks were primarily sourced from granitic rocks and a few of strongly weathered materials. These results are consistent with a previous work which suggested that the detrital zircons in the Fanjingshan Group mainly derive from the source rock dominated by granitoids (Wang et al., 2010). The Th-Sc-Zr/10 and La-Th-Sc diagrams help in the discrimination of the tectonic setting of sedimentary rock (Bhatia and Crook, 1986; Roser and Korsch, 1986). According the Th, Sc, Zr and La contents, the studied sedimentary rocks commonly plot in the continental arc field in the discrimination diagrams (Fig. 15e and f). Based on the results stated above, it is reasonable to deduce that the Taojinhe Formation was formed by the deposition of acidic rock-dominated source materials in a basin adjacent to a continental arc.

5.2.2. Source connection of the Fanjingshan granite-pegmatite suite with the Taojinhe Formation

The Neoproterozoic sedimentary basement sequences, including the Sibao, Fanjingshan, Lengjiaxi, Shuangqiaoshan, and Shangxi Groups in the JO, have similar detrital zircon age spectra with a maximum age range of ca. 880–820 Ma (e.g., Wang et al., 2007, 2014, 2010; Zhou et al., 2009; Yao et al., 2014; Li et al., 2016) and were intruded by abundant synsedimentary granitoids (870–820 Ma with a peak of 830–820 Ma) (e.g., Li et al., 2003; Wu et al., 2006; Zheng et al., 2007; Zhao et al., 2013; Wang et al., 2014; Yao et al., 2014). Up to now, numerous studies support a source connection between the basement sequences and granitoids in the JO (e.g., Li and McCulloch, 1996; Li et al., 2003; Wu et al., 2006; Wang et al., 2014; Li et al., 2016). For example, it is suggested that the Yuanbaoshan and Sanfang leucogranites and the Jiuling and Xuncun granodiorites in the southwestern and northeastern JO, were generated by the partial melting of the pelitic and psammitic protoliths in the Sibao and Shuangqiaoshan metasedimentary rocks, respectively (Li et al., 2003). The combined geochronology and geochemistry study of the Xuncun, Xiuning and Shexian granodiorites suggests that they were formed by partial melting of their host rocks which were low-maturity sedimentary rocks from the Shangxi Group (Wu et al., 2006). A comparative study of the Neoproterozoic granitoids, with their sedimentary host rocks in the JO, revealed the coupled isotope compositions among them and the geochemical variations from the eastern segment to the western segment of JO (Wang et al., 2014).

Combined with previous works (Wang et al., 2010, 2011, 2014, the results of the comparative isotope study of the Fanjingshan Group with the granite-pegmatite suite conducted as part of this study were utilized to determine the source connection between them. The result revealed that the granite-pegmatite suite has dominating $\varepsilon_{Hf}(t)$ values of 0 to −10 and T_{DM2} ages of 1700–2400 Ma overlapping with the recycling components of Paleoproterozoic crust in the Fanjingshan Group (Fig. 16a), thereby indicating a source connection. Additionally, the Taojinhe Formation mainly consists of slate, siltstone, and phyllite sourced from felsic igneous rocks and strongly weathered materials (Fig. 15a-d) with

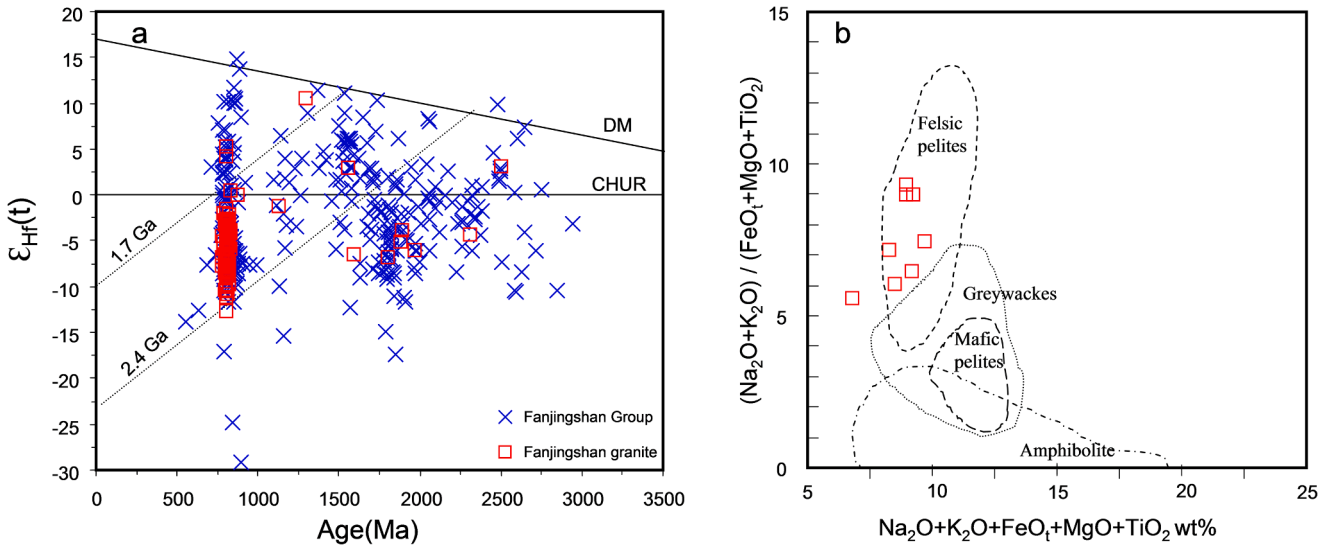

Fig. 16. Diagram of $\varepsilon_{Hf}(t)$ value versus crystallization ages of detrital zircons from the Fangjingshan Group and igneous zircons from the Fangjingshan granite (a); and source discrimination diagram for the Fangjingshan granite (b) after Sylvester (1998). Zircon data of the Fangjingshan Group and granite are from Wang et al. (2010), Wang et al. (2011), Wang et al. (2014) and this work.

lower K, Ca, Na, Mg and Fe contents than the PAAS (Fig. 7), indicating a composition similar to that of the pelites. The Fanjingshan granite has a peraluminous composition, enriched Hf isotope compositions, and low CaO/Na_2O ratios (0.06–0.15), and most samples fall in a felsic pelite source region (Fig. 16b). Moreover, the inherited zircons (1100–1900 Ma) observed in the Fanjingshan granite are comparable to some detrital zircons of the Fanjingshan Group in terms of U-Pb age and Hf isotopic composition, indicating a source contribution from the Taojinhe Formation to the Fanjingshan granite.

The RME concentrations of the Taojinhe Formation were used to evaluate the background of ore-forming elements in the Fanjingshan granite-pegmatite suite. The results show that the sedimentary rock samples from the Taojinhe Formation commonly have higher average Li (128 ppm), Sn (8 ppm), Rb (264 ppm), W (5 ppm), Ta (2 ppm), Nb (17 ppm), and Be (4 ppm) abundances than the average of the UCC by approximately 1.5–6 times. Comparatively, the Fanjingshan granite samples have higher average Li (223 ppm), Sn (44 ppm), Rb (638 ppm), W (11 ppm), Ta (9 ppm), and Nb (25 ppm) abundances than the average of the UCC by approximately 2–21 times (Fig. 17; Supplementary Table 2). Li, Sn, Rb, W, Ta, and Nb show increasing abundances, especially Sn and Ta. Be, Hf, and Zr, however, show a decreasing trend from the Taojinhe Formation to the Fanjingshan granite (Fig. 17). Notably,

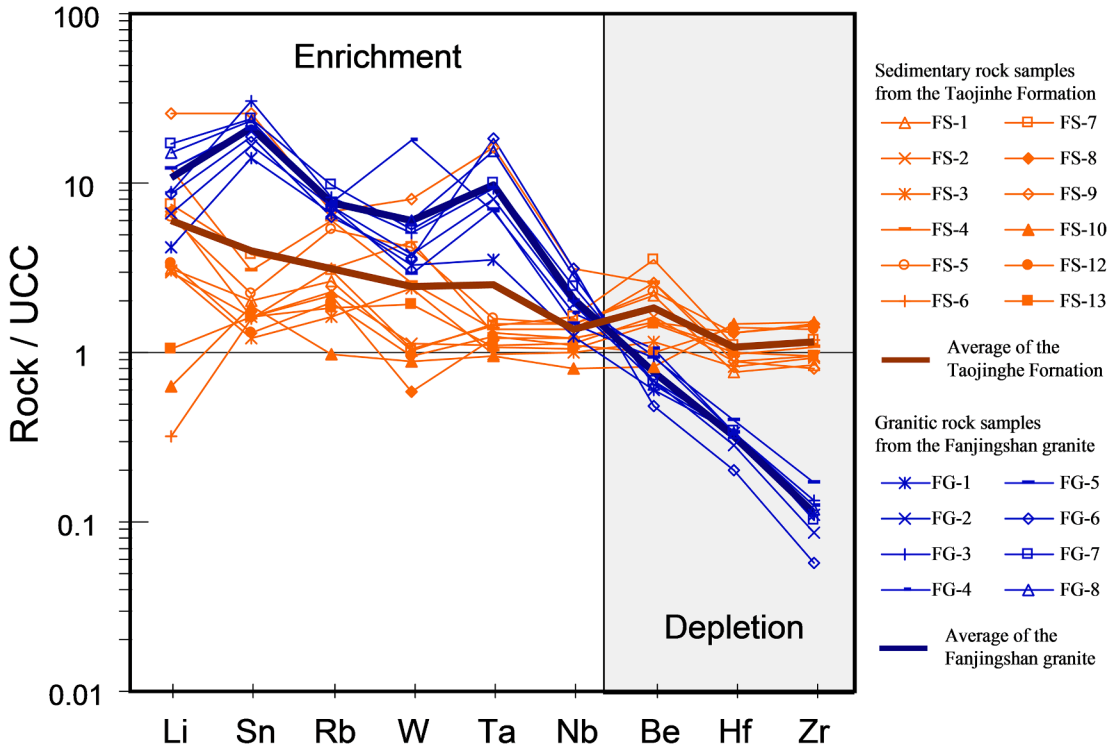

Fig. 17. Upper continental crust-normalized rare metal element patterns of the Taojinhe Formation and the granites in Fangjingshan area. Reference values of UCC are from Taylor and McLennan (1985).

sample FS-9 presents similar Li, Sn, Rb, W, Ta and Nb concentrations as those of the granite and consistent Be, Zr, and Hf concentrations as those of the other sedimentary rocks. It is reasonable to deduce that the Taojinhe Formation or similar underlying rocks (e.g., sample FS-9) can provide REMs to the Fanjingshan granite via the partial melting of clay-rich and plagioclase-poor political source indicated by the high Rb/Sr ratios (27–54, Supplementary Table 1) of the granite (e.g., Sylvester, 1998). The depletion of Be, Zr, and Hf in the Fanjingshan granite could be explained by the of presence of cordierite and zircon residuals during the partial melting of the source rocks, as indicated by the residual zircons in the Fanjingshan granite.

It is believed that the compositions of the sedimentary rock samples were negligibly modified by the nearby granite melt and the exsolution fluids from the pegmatite melt due to the four following reasons. First, the highly fractionated granitic melts commonly have eutectic components with low temperature no >700 °C (London, 2008), which restricts the interaction between the granitic melt and the cool wall rock. Second, the water–rock interactions between the exsolution fluid and wall rock are commonly characterized by tourmalinization, muscovitization, etc.; however, no evident fluid alteration or contact metamorphism was observed in the contact zone of wall rocks (Fig. 3d and e). In addition, the sedimentary rock samples in this study are primary in composition and texture without specific alteration minerals (Fig. 3m-p). The third reason is based on the Li abundances in the slate samples of FS-1, FS-2, FS-3, FS-4, and FS-7. Samples FS-1, FS-2, and FS-3 were collected from locations near granite and have low Li abundance (62–66 ppm); samples FS-4 and FS-7 were collected from locations farther away from granite and have high Li concentrations (156–253 ppm) (Supplementary Table 2). Fourth, the previous works suggested that the Li, Be, Rb, Ta, and Cs contents in the alteration haloes of wall rocks increase from the contact zone to a distance of 0.5 m, and then, gradually decrease to a low level close to the reference values at a distance of 30 m from pegmatite

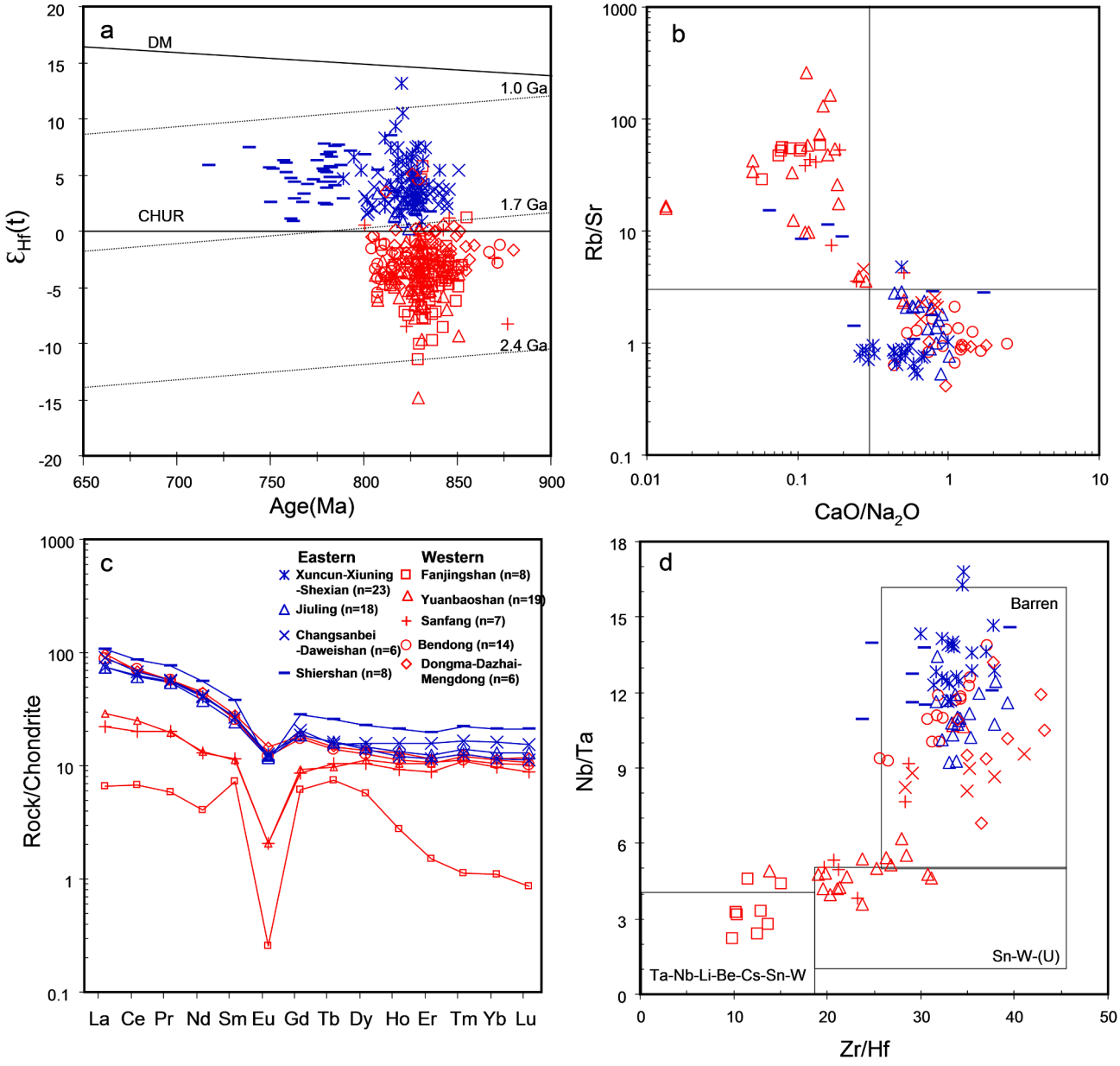

Fig. 18. Source and differentiation discrimination diagrams for the peraluminous granitoids from the eastern and western Jiangnan Orogen. Zircon $\varepsilon_{Hf}(t)$ value versus crystallization age (a) and whole rock CaO/Na_2O versus Rb/Sr (b) diagrams for source discrimination; Chondrite-normalized REE patterns (c) and whole rock Zr/Hf versus Nb/Ta diagram (d, after Ballouard et al. (2016) for differentiation discrimination. Data of the granitoids are from Li et al. (2003), Wang et al. (2010), Wang et al. (2004), (2006), (Wang et al., 2014), Wu et al., (2006), Yao et al. (2014), Zhao et al. (2013), Zheng et al. (2008) and this work.

(Chen et al., 2016; Zhao et al., 2017).

5.3. Ore forming potential of the Neoproterozoic granitoids in the Jiangnan Orogen

According to the classical model (Černý, 1991); Černý et al., 2012a, 2012b), S-type granites formed during orogeny (particularly late- to post-orogenic stages) facilitate the formation of Li-, Cs- and Ta-rich pegmatite. Previous studies suggested that abundant Neoproterozoic S-type granitoids (ca. 830–800 Ma) formed in the post-collisional stage during orogeny (e.g., Wu et al., 2006; Zheng et al., 2007; Zhao et al., 2011; Wang et al., 2014, 2017), however, only the Fanjingshan granite-pegmatite suite with Sn-Ta-Nb mineralization has been demonstrated till date. Therefore, the Fanjingshan granite is set as an ore-forming standard to evaluate the ore forming potential of the synchronous S-type granitoids in the JO based on a comparative geochemistry study.

According to the data obtained in this study, the granitoids in the eastern JO commonly have positive $\varepsilon_{Hf}(t)$ values of 0 - +9 and T_{DM2} ages of 1.1–1.7 Ga. In contrast, the granitoids in the western JO generally have negative $\varepsilon_{Hf}(t)$ values and T_{DM2} ages of 0 to −11 and 1.7 to 2.4 Ga, respectively (Fig. 18a). The isotope diversity indicates that the granitoids have distinct sources from the basement sequences (or their lower equivalents). According to previous studies, the basement sequences in the eastern JO (such as the Xikou and Shuangqiaoshan Groups) were sourced primarily from the Shuangxiwu arc terrane and mixed with materials from the central Yangtze Block. The Fanjingshan and Sibao Groups in the western JO, however, have multiple sources from the Yangtze and Cathaysia blocks and the Shuangxiwu arc (e.g., Wang et al., 2014; Li et al., 2016). Therefore, it is reasonable to deduce that the granitoids sources in the eastern and western JO are dominated by juvenile materials from the Shuangxiwu arc and the ancient crust materials from Yangtze and Cathaysia Blocks, respectively. In addition, the source diversity is also reflected by the CaO/Na_2O and Rb/Sr ratios of the whole rock. The Fanjingshan, Yuanbaoshan and Sanfang granites in the western JO generally show low CaO/Na_2O (<0.3) and high Rb/Sr ratios (>3). In contrast, the Bendong granite and other granitoids in the eastern JO all have high CaO/Na_2O (>0.3) and low Rb/Sr ratios (<3) (Fig. 18b), indicating pelite- and psammite-derived peraluminous melts, respectively (e.g., Sylvester, 1998; Li et al., 2003).

In differentiation, the Fanjingshan, Yuanbaoshan and Sanfang granites are distinct from other granitoids owing to their low REEs concentrations, strongly negative Eu anomalies, and tetrad effects on the REE patterns (Fig. 18c). Additionally, the granitoids have lower Nb/Ta (<6) and Zr/Hf (<30) ratios than those of other granitoids in the eastern JO (Fig. 18d). These features indicate that the Fanjingshan, Yuanbaoshan, and Sanfang granites have experienced intense fluid-melt interaction and high degree of differentiation (e.g., Irber, 1999; Ballouard et al., 2016); therefore, it can be concluded that the Neoproterozoic granitoids in the eastern JO are insufficient to produce pegmatite or enrich RMEs. They are barren and similar to the synorogenic peraluminous granitoids in the Chinese Altai. Although they have a huge advantage in quantity, they are limited by their immature source and low degree of differentiation (Lv et al., 2018). The Yuanbaoshan and Sanfang granites have similar sources to the Fanjingshan granite (Fig. 18a and b), but they lack sufficient differentiation as the latter (Fig. 18c and d), they could be the enriching source of Sn and W. The Bendong, Dongma, Dazhai, Longyou, Mengdong, and Zhaigun granites show a similar source to that of the Fanjingshan granite (Fig. 18a) but have different protolith lithology and differentiation (Fig. 18c-e), indicating limited potential as the enriching source of rare metals. Considering of the rare metal-rich clay rocks worldwide, clay mineral-rich pelite could be significant for the generation of the peraluminous rare metal granite and pegmatite.

5.4. Implications for rare-metal mineralization in South China

Abundant Paleozoic and Mesozoic Nb-Ta ± Sn-W ± Be-Li ore deposits have been found in South China, which are associated with Li-F granite (e.g., Yichun Ta-Nb-Li deposit, (Yin et al., 1995); pegmatite (e.g., Renli Ta-Nb-Be-Li deposit, Li et al., 2020), and aplite, with CGM U-Pb ages from the Late Silurian to Late Cretaceous (e.g., Che et al., 2019). The Nb-Ta ore deposits with reported Hf isotope compositions were collected for source study (Table 2) and the results showed that all the Nb-Ta ore deposits associated with peraluminous granite and pegmatite have similar Hf isotope compositions to those of the Fanjingshan rare metal granite-pegmatite suite, with T_{DM} model ages ranging from 1.6 Ga to 2.3 Ga (Fig. 19). This indicates that (1) the sources of Nb-Ta ore deposits in South China could primarily be derived from the Paleoproterozoic crust and (2) the western JO has more affinity to the Cathaysia Block regarding the source and metallogenic characteristics. For the first point, the ore deposits dominated by Nb-Ta mineralization exhibited increasing scales with time, and peaked during the Jurassic Period (Table 2). In addition, the Mesozoic Nb-Ta ore deposits are commonly associated with the latest phases of composite plutons, such as the Nb-Ta ore deposits in Yashan and Mufushan composite plutons (e.g., Yang et al., 2014; (Li et al., 2019)). Therefore, it is reasonable to deduce that the metallogenic peak of Nb-Ta ore in Mesozoic is associated with the gradual enrichment of Nb and Ta caused by multiple reworkings of the Paleoproterozoic crust. Similarly, the Mesozoic Sn-W mineralized granites in South China are suggested to form by the re-melting of the granulitic residues in the lower crust after extraction of early granites from the same source region (e.g., (Chen et al., 2014)). For the second point, previous studies have suggested that the Fanjingshan and Sibao Groups may contain a certain amount of ancient materials from the Cathaysia Block (e.g., Wang et al., 2014). Considering metallogenic characteristics, the Yangtze Craton abounds with large-scale low-temperature Pb-Zn, Au-Hg-Sb-As, and An-Sb mineralizations during the Phanerozoic (e.g., Hu et al., 2020), and the Cathaysia Block is characterized by multiple generations of Nb-Ta ± Sn-W mineralization (e.g., Che et al., 2019)due to the source constraints from diverse Precambrian basements (e.g., (Ma, 2008); Hu et al., 2020).

6. Conclusions

(1) The geology, mineralogy, bulk composition, chronology and isotope studies prove the spatial–temporal and source-differentiation relationships between the Fanjingshan granite and adjacent pegmatites, indicating a genetic relationship between them and the existence of the Neoproterozoic rare metal granite-pegmatite suite in the JO.

(2) The petrography and whole-rock composition studies of the Taojinhe Formation, which is the host rock of the Fanjingshan granite-pegmatite suite, reveal that the formation contains mature and immature source materials from acidic igneous rocks and was deposited in a continental arc setting. A comparison of the Hf isotope compositions of the granite-pegmatite suite with those of the Fangjingshan Group and the high Li, Sn, Rb, W, Ta, and Nb background concentrations in the Taojinhe Formation support the conclusion that the formation was contributing source to the granite-pegmatite suite.

(3) A comparative study of the Fanjingshan granite with the synchronous S-type granitoids reveals that the granitoids in the eastern and western JO have distinct sources and degrees of differentiation, indicating the limited ore-forming potential of the Neoproterozoic granitoids in the eastern JO.

(4) The Fanjingshan rare-metal granite-pegmatite suite has consistent Hf isotope model ages of 1.6–2.3 Ga with the Paleozoic and Mesozoic Nb-Ta ± Sn-W ± Be-Li ore deposits in South China, indicating the ore-forming source from the Paleoproterozoic crust

Table 2
The zircon U-Pb age and Hf isotope compositions of rare metal ore deposits in South China

Ore field	Host rock	Tectonic location	Mineralization	Scale	Age (Ma)	$\varepsilon_{(Hf)}t$	$T_{DM}c$ (Ma)	References
Fangjingshan	Pegmatite	Jiangnan Orogen	Ta-Nb-Sn	Small	Ca. 830	+1.13–−9.51	1650–2310	This work
Xigang	Pegmatite	Wuyi-Yunkai Orogen	Ta-Nb-Li	Small	Ca. 420	−3.2–13.7	1602–2258	Che et al., 2019; Cui et al., 2013
Nanping	Pegmatite		Ta-Nb-Sn	Medium-large	Ca. 390	−11.6–−13.8	2107–2246	Tang et al., 2017
Limu	Granite-pegmatite	Qin-Hang metallogenic belt	Ta-Nb-Sn-W	Large	203–227	−5.79–−14.6	1618–2171	Huang et al., 2020
Gedongping	Pegmatite-aplite		Sn-Nb-Ta-Be	Small	153 ± 3	−7.2–−11.3	1650–1910	Tian et al., 2020
Yichun	Granite		Ta-Nb-Sn-Li	Supra large	150 ± 1.4	+0.7–−14.1	1150–2080	Yang et al., 2014
Renli	Pegmatite	Jiangnan Orogen	Ta-Nb-Be-Li	Supra large	133 ± 2.6	−5.4–−10.8	1537–1877	Li et al., 2020

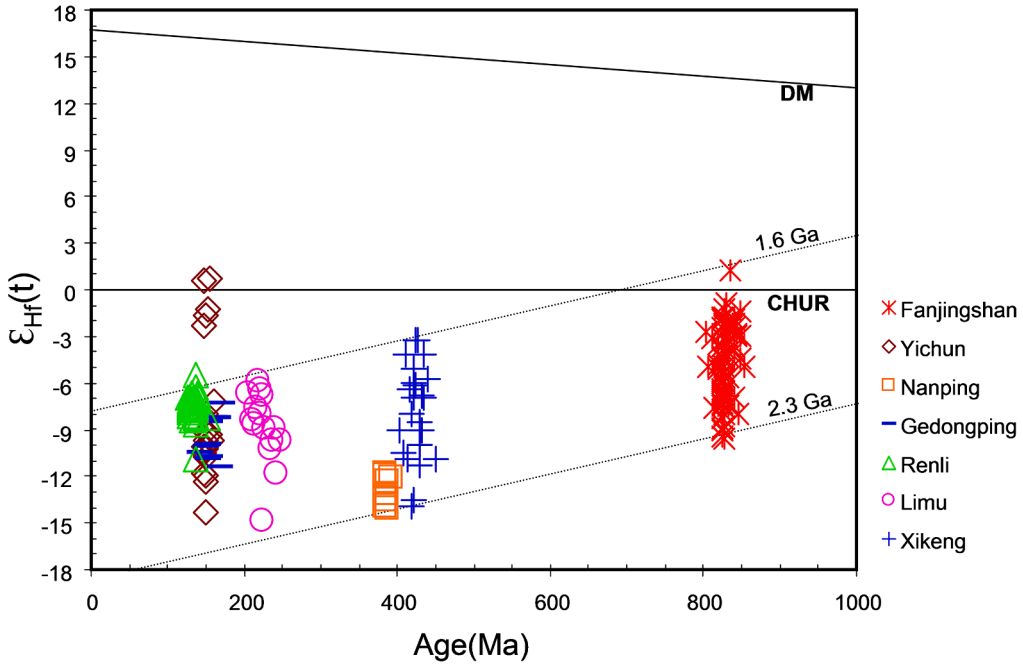

Fig. 19. Zircon $\varepsilon_{Hf}(t)$ value versus crystallization age diagram, with showing the source connection of the Fanjingshan granite-pegmatite suite with the Paleozoic-Mesozoic rare metal granites, pegmatites and aplites in South China. Data are from Cui et al. (2013), Huang et al. (2020), Li et al. (2020), Tang et al. (2017), Tian et al. (2020), Yang et al. (2014) and this work.

and the source inheritance of the western JO from the Cathaysia Block.

Declaration of Competing Interest

The authors declare that they have no known competing financial interests or personal relationships that could have appeared to influence the work reported in this paper.

Acknowledgements

This study is jointly supported by the National Science Foundation of China (Grants Nos. 41873030 and 41403016), the Strategic Priority Research Program (B) of the Chinese Academy of Sciences (XDB18000000) and the Science and Technology Agency of Guizhou province, China (Grant Nos. J[2015]2142 and [2020]1Y170). Drs. Yan-Wen Tang, Zhi-Hui Dai, You-Wei Chen and Shao-Hua Dong, and Engineers Wen-Qin Zheng and Xiang Li are appreciated for their laboratory assistance. Editor-In-Chief Franco Pirajno, Assoc. Editor Harald G. Dill and two anonymous reviewers are appreciated for their constructive comments to improve this manuscript and hard works during the epidemic.

Appendix A. Supplementary data

Supplementary data to this article can be found online at https://doi.org/10.1016/j.oregeorev.2020.103923.

References

Abedini, A., Calagari, A.A., Azizi, M.R., 2018. The tetrad-effect in rare earth elements distribution patterns of titanium-rich bauxites: Evidence from the Kanigorgeh deposit, NW Iran. J. Geochem. Explor. 186, 129–142.
Ballouard, C., Poujol, M., Boulvais, P., Branquet, Y., Tartese, R., Vigneresse, J.L., 2016. Nb-Ta fractionation in peraluminous granites: a marker of the magmatic-hydrothermal transition. Geology 44, 231–234.
Bhatia, M.R., Crook, K.A.W., 1986. Trace element characteristics of graywackes and tectonic setting discrimination of sedimentary basins. Contrib. Mineral. Petrol. 92, 181–193.
BGGZP (Bureau of Geology of Guizhou Province), 1962. Report of magmatic rocks and rare metal minerals in Fanjingshan area of Yinjiang county, Guizhou province. pp. 1–66 (in Chinese).
BGMRGZP (Bureau of Geology and Mineral Resources of Guizhou Province), 1987. Regional Geology of Guizhou Province. Geological Publishing House, Beijing (in Chinese with English abstract).
BGMRGXP (Bureau of Geology and Mineral Resources of Guangxi Province), 1985. Regional Geology of Guangxi Province. Geological Publishing House, Beijing (in Chinese with English Abstract).
Černý, P., 1991. Rare-element granite pegmatites. Part I: anatomy and internal evolutionof pegmatite deposits. Geosci. Can. 18, 49–67.

Černý, P., 1991. Rare-element granitic pegmatites. Part II: regional to global environments and petrogenesis. Geosci. Can. 18, 68–81.
Černý, P., Ercit, T.S., 2005. The classification of granitic pegmatites revisited. Can. Mineral. 43, 2005–2026.
Černý, P., Halden, N.M., Ferreira, K., Meintzer, R.E., Brisbin, W.C., Chackowsky, L.E., Corkery, M.T., Longstaffe, F.J., Trueman, D.L., 2012a. Extreme fractionation and deformation of the leucogranite-pegmatite suite at Red Cross lake, Manitoba, Canada. II. Petrology of the leucogranites and pegmatites. Can. Mineral. 50, 1807–1822.
Černý, P., London, D., Novák, M., 2012b. Granitic pegmatites as reflections of their sources. Elements 8, 289–294.
Černý, P., Meintzer, R.E., 1988. Fertile granites in the Archean and Proterozoic fields of rare-element pegmatites: crustal environment, geochemistry and petrogenetic relationships. In: Taylor, R.P., Strong, D.F. (Eds.), Recent Advances in the Geology of Granite-Related Mineral Deposits, Canadian Institute of Mining and Metallurgy Special Publication 39, pp. 170–206.
Che, X.D., Wang, R.C., Wu, F.Y., Zhu, Z.Y., Zhang, W.L., Hu, H., Xie, L., Lu, J.J., Zhang, D., 2019. Episodic Nb-Ta mineralisation in South China: Constraints from in situ LA–ICP–MS columbite-tantalite U-Pb dating. Ore Geol. Rev. 105, 71–85.
Chen, B., Ma, X., Wang, Z., 2014. Origin of the fluorine-rich highly differentiated granites from the qianlishan composite plutons (south china) and implications for polymetallic mineralization. J. Asian Earth Sci. 93 (15), 301–314.
Chen, Y., Zhang, H., Zhao, J.Y., 2016. Altered country rocks of No. 807 pegmatite vein in the Kaluan ore area, Xinjiang: ore-forming element diffusion model and its influencing factors. Geochimica 45 (3), 268–280 (in Chinese with English abstract).
Chen, Y.W., Hu, R.Z., Bi, X.W., Luo, J.C., 2019. Genesis of the Guangshigou pegmatite-type uranium deposit in the North Qinling Orogenic Belt, China. Ore Geol. Rev. 115, 103165.
Cheng, H., 1993. Geochemistry of Proterozoic island-arc volcanic rocks in northwest Zhejiang. Geochimica 1, 18–27 (in Chinese with English abstract).
Condie, K.C., 1993. Chemical composition and evolution of the upper continental crust: contrasting results from surface samples and shales. Chem.Geol. 104, 1–37.
Cox, R., Lowe, D.R., Cullers, R.L., 1995. The influence of sediment recycling and basement composition on evolution of mudrock chemistry in the southwestern United States. Geochim. Cosmochim. Ac. 59, 2919–2940.
Cui, Y.Y., Zhao, Z.D., Jiang, T., Yang, J.B., Ding, C., Sheng, D., et al., 2013. Geochronology, geochemistry and petrogenesis of the Early Paleozoic granitoids in southern Jiangxi Province, China (in Chinese with English abstract). Acta Petrol. Sin 29 (11), 4011–4024.
Dill, H.G., 2015. The Hagendorf-Pleystein Province: the center of pegmatites in an ensialic orogen. Springer 15, 1–465.
Dill, H.G., 2015. Pegmatites and aplites: Their genetic and applied ore geology. Ore Geol. Rev. 69, 417–561.
Dill, H.G., 2016. The CMS classification scheme (Chemical composition-Mineral assemblage-Structural geology)-linking geology to mineralogy of pegmatitic and aplitic rocks. Neues Jahrbuch für Mineralogie-Abhandlungen: J. Mineral. Geochem. 193 (3), 231–263.
Elhlou, S., Belousova, E., Griffin, W.L., Pearson, N.J., O'Reilly, S.Y., 2006. Trace element and isotopic composition of GJ-red zircon standard by laser ablation. Geochim. Cosmochim. Ac. 70 (18), A158.
Fedo, C.M., Nesbitt, H.W., Young, G.M., 1995. Unraveling the effects of potassium metasomatism in sedimentary rocks and paleosoils, with implications for paleoweathering conditions and provenance. Geology 23, 921–924.
Floyd, P.A., Leveridge, B.E., 1987. Tectonic environment of the Devonian Gramscatho basin, south Cornwall: framework mode and geochemical evidence from turbiditic sandstones. J. Geol. Soc. London 144, 531–542.
Floyd, P.A., Winchester, J.A., Park, R.G., 1989. Geochemistry and tectonic setting of Lewisian clastic metasediments from the early Proterozoic Lock Marie Group of Gairlock, Scotland. Precamb. Res. 45, 203–214.
Gao, J., Klemd, R., Long, L.L., Xiong, X.M., Qian, Q., 2009. Adakitic signature formed by ractional crystallization: an interpretation for the Neo-Proterozoic meta-plagio granites of the NE Jiangxi ophiolitic mélange belt, South China. Lithos 110, 277–293.
Gao, S., Ling, W.L., Qiu, Y.M., Lian, Z., Hartmann, G., Simon, K., 1999. Contrasting geochemical and Sm-Nd isotopic compositions of Archean metasediments from the Kongling high-grade terrain of the Yangtze craton: evidence for cratonic evolution and redistribution of REE during crustal anatexis. Geochim. Cosmochim. Acta 63, 2071–2088.
Gillespie, M., Styles, M., 1999. BGS rock classification scheme. Classification of igneous rocks 1.
Griffin, W.L., Pearson, N.J., Belousova, E.A., Saeed, A., 2006. Comment: Hf-isotope heterogeneity in zircon 91500. Chem. Geol. 233 (3–4), 358–363.
Hao, X.F., Fu, X.F., Liang, B., Yuan, L.P., Pan, M., Tang, Y., 2015. Formation ages of granite and X03 pegmatite vein in Jiajika, western Sichuan, and their geological significance. Mineral Deposits 34 (6), 1199–1208 (in Chinese with English abstract).
Hou, L.J., 2018. The comparative study of diagenetic, metallogenic characteristics and tectonic environment of two kinds of pegmatites in China. A dissertation submitted to Chinese Academy of Geological Sciences for doctoral degree, Beijing, pp. 1–169 (in Chinese with English abstract).
Hu, R.Z., Chen, W., Bi, X.W., Fu, S.L., Yin, R.S., Xiao, J.F., 2020. Control of the Precambrian basement on the formation of the Mesozoic large-scale low-temperature mineralization in the Yangtze Craton. Earth Sci. Front. 27 (2), 137–150 (in Chinese with English abstract).
Huang, W.T., Wu, J., Liang, H.Y., Zhang, J., Ren, L., Chen, X.L., 2020. Ages and genesis of W-Sn and Ta-Nb-Sn-W mineralization associated with the Limu granite complex, Guangxi, China. Lithos 352–353, 105321.
Hulsbosch, N., Hertogen, J., Dewaele, S., André, L., Muchez, P., 2014. Alkali metal and rare earth element evolution of rock-forming minerals from the gatumba area pegmatites (Rwanda): quantitative assessment of crystal-melt fractionation in the regional zonation of pegmatite groups. Geochim. Cosmochim. Acta 132, 349–374.
Irber, W., 1999. The lanthanide tetrad effect and its correlation with K/Rb, Eu/Eu*, Sr/Eu, Y/Ho, and Zr/Hf of evolving peraluminous granite suites. Geochim. Cosmochim. Acta 63, 489–508.
Joo, Y.J., Lee, Y., Bai, Z.Q., 2005. Provenance of the Qingshuijian Formation (Late Carboniferous), NE China: implications for tectonic processes in the northern margin of the North China block. Sedim. Geol. 177 (1–2), 97–114.
Kinny, P.D., Maas, R., 2003. Lu-Hf and Sm-Nd isotope systems in zircon. Rev. Mineral. Geochem. 53 (1), 327–341.
Li, J.Y., Wang, X.L., Zhang, F.F., Zhou, X.H., Shu, X.J., 2016. A rhythmic source change of the Neoproterozoic basement meta-sedimentary sequences in the Jiangnan Orogen: Implications for tectonic evolution on the southeastern margin of the Yangtze Block. Precamb. Res. 280, 46–60.
Li, P., Li, J.K., Liu, X., Li, C., Huang, Z.B., Zhou, F.C., 2019. Geochronology and source of the rare-metal pegmatite in the Mufushan area of the Jiangnan Orogenic belt: a case study of the giant Renli Nb-Ta deposit in Hunan, China. Ore Geol. Rev. 116, 103237.
Li, X.H., Li, W.X., Li, Z.X., Lo, C.H., Wang, J., Ye, M.F., Yang, Y.H., 2009. Amalgamation between the yangtze and cathaysia blocks in south china: constraints from shrimp u-pb zircon ages, geochemistry and nd-hf isotopes of the shuangxiwu volcanic rocks. Precamb. Res. 174 (1–2), 117–128.
Li, X.H., Li, Z.X., Ge, W.C., Zhou, H.W., Li, W.X., Liu, Y., Wingate, M.T.D., 2003. Neoproterozoic granitoids in South China: crustal melting above a mantle plume at ca. 825 Ma? Precamb. Res. 122, 45–83.
Li, X.H., McCulloch, M.T., 1996. Secular variation in the Nd isotopic composition of Neoproterozoic sediments from the southern margin of the Yangtze Block: evidence for a Proterozoic continental collision in southeast China. Precamb. Res. 76, 67–76.
Li, X.H., Zhou, G.Q., Zhao, J.X., Fanning, C.M., Compston, W., 1994. SHRIMP ion microprobe zircon U-Pb age and Sm-Nd isotopic characteristics of the NE Jiangxi ophiolite and its tectonic implications. Chin. J. Geochem. 13, 317–325.
Liu, Y.S., Hu, Z.C., Gao, S., Günther, D., Xu, J., Gao, C.G., Chen, H.H., 2008. In situ analysis of major and trace elements of anhydrous minerals by la-icp-ms without applying an internal standard. Chem. Geol. 257 (1), 34–43.
Lonndon, D., 2008. Pegmatites. Can. Mineral. Special Publication 10, 1-347.
London, D., 2014. A petrologic assessment of internal zonation in granitic pegmatites. Lithos 184–187, 74–104.
Ludwig, K.R., 2003. User's manual for Isoplot/Ex, Version 3. 00. A Geochronological Toolkit for Microsoft Excel: Berkeley Geochronology Center Special Publication 4, 1–70.
Lv, Z.H., Zhang, H., Tang, Y., Guan, S.J., 2012. Petrogenesis and magmatic-hydrothermal evolution time limitation of Kelumute No. 112 pegmatite in Altay, Northwestern China: evidence from zircon U-Pb and Hf isotopes. Lithos 154, 374–391.
Lv, Z.H., Zhang, H., Tang, Y., Liu, Y.L., Zhang, X., 2018. Petrogenesis of syn-orogenic rare metal pegmatites in the Chinese Altai: evidences from geology, mineralogy, zircon U-Pb age and Hf isotope. Ore Geol. Rev. 95, 161–181.
Ma, D.S., 2008. Metallogenetic characteristics of the important deposits in South China. Bull. Mineral. Petrol. Geochem. 27 (3), 209–217 (in Chinese with English abstract).
Ma, Z.L., Zhang, H., Tang, Y., Lv, Z.H., Zhang, X., Zhao, J.Y., 2015. Zircon U-Pb geochronology and Hf isotopes of pegmatites from the Kaluan mining area in the Altay, Xinjiang and their genetic relationship with the Halong granite. Geochimica 44, 9–26 (in Chinese with English abstract).
McCauley, A., Bradley, D.C., 2014. The global age distribution of granitic pegmatites. Can. Mineral. 52 (2), 183–190.
Müller, A., Romer, R.L., Pedersen, R.B., 2017. The Sveconorwegian Pegmatite Province - Thousands of pegmatites without parental granites. Can. Mineral. 55, 283–315.
Nesbitt, H.W., Young, G.M., 1984. Prediction of some weathering trends of plutonic and volcanic rocks based on thermodynamics and kinetic considerations. Geochim. Cosmochim. Ac. 48, 1523–1534.
Roser, B.P., Korsch, R.J., 1986. Determination of tectonic setting of sandstone-mudstone suites using SiO_2 content and K_2O/Na_2O ratio. J. Geol. 94, 635–650.
Selway, J.B., Breaks, F.W., Tindle, A.G., 2005. A review of rare-element (Li-Cs-Ta) pegmatite exploration techniques for the Superior Province, Canada, and large worldwide tantalum deposits. Explor. Mining Geol. 14, 1–30.
Shand, S.J., 1948. Eruptive rocks: their genesis, composition, classification, and their relation to ore deposits with a chaper on meteorites. J. Geol. 56 (6), 593.
Shaw, D.M., 1968. A review of K-Rb fractionation trends by covariance analysis. Geochim. Cosmochim. Ac. 32, 573–602.
Shaw, R.A., Goodenough, K.M., Roberts, N.M.W., Horstwood, M.S.A., Chenery, S.R., Gunn, A.G., 2016. Petrogenesis of rare-metal pegmatites in high-grade metamorphic terranes: a case study from the Lewisian Gneiss Complex of north-west Scotland. Precamb. Res. 281, 338–362.
Shu, L.S., Faure, M., Jiang, S.Y., Yang, Q., Wang, Y.J., 2006. SHRIMP zircon U-Pb age, litho- and biostratigraphic analyses of the Huaiyu Domain in South China - Evidence for a Neoproterozoic orogen, not Late Paleozoic-Early Mesozoic collision. Episodes 29 (4), 244–252.
Shu, L.S., Zhou, G.Q., Shi, Y.S., Yin, J., 1994. Study on the high pressure metamorphic blueschist and its late Proterozoic age in the Eastern Jiangnan belt. Chin. Sci. Bull. 39, 1200–1204.
Simmons, W.B., Falster, A.U., 2016. Evidence for an Anatectic Origin of an LCT Type Pegmatite: Mt. Foord Pegmatite Symposium, Mica, Maine, In Second Eugene E, p. 103.
Sun, J.J., Shu, L.S., Santosh, M., Wang, L.S., 2017. Neoproterozoic tectonic evolution of the Jiuling terrane in the central Jiangnan orogenic belt (South China): Constraints from magmatic suites. Precamb. Res. 302, 279–297.

Sun, S.S., McDonough, W.F. 1989. Chemical and isotopic systematics of oceanic basalts: implications for mantle composition and processes. In: Saunders A.D., Norry M.J., (Eds.), Magmatism in Ocean Basins. Geological Society, London. Special Publications 42, pp. 313–345.
Sylvester, P.J., 1998. Post-collisional strongly peraluminous granites. Lithos 45, 29–44.
Tang, Y., Zhao, J.Y., Zhang, H., Cai, D.W., Lv, Z.H., Liu, Y.L., Zhang, X., 2017. Precise columbite-(Fe) and zircon U-Pb dating of the Nanping No. 31 pegmatite vein in northeastern Cathaysia Block, SE China. Ore Geol. Rev. 83, 300–311.
Taylor, S.R., McLennan, S.M., 1985. The continental crust: its composition and evolution. Blackwell Scientific Publications, Oxford, UK, p. 312.
Tian, E.N., Wang, R.C., Xie, L., Zhang, W.L., Che, X.D., Zhang, R.Q., 2020. Mineralogy and geochemistry of the newly discovered Late Mesozoic granite-pegmatite and associated Sn-Nb-Ta-Be mineralization in the Miao'ershan-Yuechengling composite batholith, northern Guangxi, South China. J. Asian Earth Sci. 190, 104149.
Tkachev, A.V., 2011. Evolution of metallogeny of granitic pegmatites associated with orogens throughout geological time. Geol. Soc. Lond. Spec. Publ. 350, 7–23.
Trueman, D. L., Černý, P., 1982. Exploration for rare element granitic pegmatites. In: Granitic Pegmatites in Science and Industry. Mineralogical Association of Canada Short Course Handbook, Vol. 8 (Černý, P., ed.), pp. 463–493.
Van de Kamp, P.C., Leake, B.E., 1985. Petrography and geochemistry of feldspathic and mafic sediments of the northeastern Pacific margin. Trans. R. Soc. Edinb. Earth Sci. 76, 411–499.
Wang, L.J., Griffin, W.L., Yu, J.H., O'Reilly, S.Y., 2010. Precambrian crustal evolution of the Yangtze Block tracked by detrital zircons from Neoproterozoic sedimentary rocks. Precamb. Res. 177 (1), 131–144.
Wang, M., Dai, C.G., Chen, J.S., Wang, X.H., Ma, H.Z., 2011. In-situ zircon geochronology and Hf isotope of muscovite-bearing leucogranites from Fanjingshan, Guizhou Province, and constraints on continental growth of the Southern China block. Earth Sci. Front. 18 (5), 213–223 (in Chinese with English abstract).
Wang, M., Dai, C.G., Chen, J.S., Wang, X.H., Ma, H.Z., 2016. Neoproterozoic geochronologic framework of magmatism in Fanjingshan area and its tectonic implications. Geol. China 43 (3), 843–856 (in Chinese with English abstract).
Wang, T., Tong, Y., Jahn, B.M., Zou, T.R., Wang, Y.B., Hong, D.W., Han, B.F., 2007. SHRIMP U-Pb Zircon geochronology of the Altai No. 3 Pegmatite, NW China, and its implications for the origin and tectonic setting of the pegmatite. Ore Geol. Rev. 32, 325–336.
Wang, X.L., Zhou, J.C., Chen, X., Zhang, F.F., Sun, Z.M., 2017. Formation and evolution of the Jinagnan Orogen. Bull. Mineral. Petrol. Geochem. 36 (5), 714–734 (in Chinese with English abstract).
Wang, X.L., Zhou, J.C., Griffin, W.L., Wang, R.C., Qiu, J.S., O'Reilly, S.Y., Xu, X.S., Liu, X. M., Zhang, G.L., 2007. Detrital zircon geochronology of Precambrian basement sequences in the Jiangnan orogen: dating the assembly of the Yangtze and Cathaysia Blocks. Precamb. Res. 159, 117–131.
Wang, X.L., Zhou, J.C., Griffin, W.L., Zhao, G.C., Yu, J.H., Qiu, J.S., Zhang, Y.J., Xing, G. F., 2014. Geochemical zonation across a Neoproterozoic orogenic belt: Isotopic evidence from granitoids and metasedimentary rocks of the Jiangnan orogeny, China. Precamb. Res. 242, 154–171.
Wang, X.L., Zhou, J.C., Qiu, J.S., Gao, J.F., 2004. Geochemistry of the Meso- to Neoproterozoic basic-acid rocks from Hunan Province, South China: implications for the evolution of the western Jiangnan orogen. Precamb. Res. 135, 79–103.
Wang, X.L., Zhou, J.C., Qiu, J.S., Zhang, W.L., Liu, X.M., 2006. LA-ICP-MS U-Pb zircon geochronology of the Neoproterozoic igneous rocks from Northern Guangxi, South China: implications for tectonic evolution. Precamb. Res. 145, 111–130.
Wiedenbeck, M., Hanchar, J.M., Peck, W.H., Sylvester, P., Valley, J., Whitehouse, M., Kronz, A., Morishita, Y., Nasdala, L., Fiebig, J., Franchi, I., Giard, J.P., Greenwood, R.C., Hinton, R., Kita, N., Mason, P.R.D., Norman, M., Ogasawara, M., Piccoli, P.M., Rhede, D., Satoh, H., Schulz-Dobrick, B., Skar, O., Spicuzza, M.J., Terada, K., Tindle, A., Togashi, S., Vennemann, T., Xie, Q., Zheng, Y.F., 2004. Further characterisation of the 91500 zircon crystal. Geostand. Geoanal. Res. 28, 9–39.
Wu, G.Y., Fu, H.Q., Tang, J.F., 1998. Features and tectonic setting of the Late Proterozoic Dengshan Group volcanic in northeastern Jiangxi area. Acta Petrol. Sin. 14 (2), 240–250 (in Chinese with English abstract).
Wu, R.X., Zheng, Y.F., Wu, Y.B., Zhao, Z.F., Zhang, S.B., Liu, X.M., Wu, F.Y., 2006. Reworking of juvenile crust: element and isotope evidence from neoproterozoic granodiorite in south China. Precam. Res. 146 (3–4), 179–212.
Yan, Q.H., Qiu, Z.W., Wang, H., Wang, M., Wei, X.P., Li, P., Zhang, R.Q., Li, C.Y., Liu, J. P., 2018. Age of the Dahongliutan rare metal pegmatite deposit, West Kunlun, Xinjiang (NW China): constraints from LA-ICP-MS U-Pb dating of columbite-(Fe) and cassiterite. Ore Geol. Rev. 100, 561–573.
Yang, S.F., Gu, M.G., Lu, C.Z., 2009. Geochemical characteristics and tectonic implications of the island-arc volcanic rocks of Mesoproterozoic in Zhangcun, Zhejiang Province. J. Jilin Univ. (Earth Science Edition) 39 (4), 689–698 (in Chinese with English abstract).
Yang, Z.L., Qiu, J.S., Xing, G.F., Yu, M.G., Zhao, J.L., 2014. Petrogenesis and magmatic evolution of the granite pluton in Yinchun, Jiangxi Province, and their constraints on mineralization. Acta Geol. Sin. 88 (5), 850–868 (in Chinese with English abstract).
Yao, J.L., Cawood, P.A., Shu, L.S., Li, J.Y., 2016. An early Neoproterozoic Accretionary Prism Ophiolitic Mélange from the Western Jiangnan Orogenic Belt, South China. J. Geol. 124 (5), 587–601.
Yao, J.L., Cawood, P.A., Shu, L.S., Zhao, G.C., 2019. Jiangnan Orogen, South China: A ~970-820 Ma Rodinia margin accretionary belt. Earth-Sci. Rev. 196, 102872.
Yao, J.L., Shu, L.S., Santosh, M., Zhao, G.C., 2014. Neoproterozoic arc-related mafic-ultramafic rocks and syn-collision granite from the western segment of the Jiangnan Orogen, South China: constraints on the Neoproterozoic assembly of the Yangtze and Cathaysia Blocks. Precamb. Res. 243, 39–62.
Yin, C., Lin, S., Davis, D.W., Xing, G., Davis, W.J., Cheng, G., Xiao, W., Li, L., 2013. Tectonic evolution of the southeastern margin of the Yangtze Block: Constraints from SHRIMP U-Pb and LA-ICP-MS Hf isotopic studies of zircon from the eastern Jiangnan Orogenic Belt and implications for the tectonic interpretation of South China. Precamb. Res. 236, 145–156.
Yin, L., Pollard, P.J., Hu, S.X., Taylor, R.G., 1995. Geologic and geochemical characteristics of the Yichun Ta-Nb-Li deposit, Jiangxi Province, South China. Econ. Geol. 90, 577–585.
Zagorsky, V.Y., Vladimirov, A.G., Makagon, V.M., Kuznetsova, L.G., Smirnov, S.Z., D'yachkov, B.A., Annikova, I.Y., Shokalsky, S.P., Uvarov, A.N., 2014. Large fields of spodumene pegmatites in the settings of rifting and postcollisional shear-pull-apart dislocations of continental lithosphere. Russ. Geol. Geophys. 55, 237–251.
Zhai, M.G., Wu, F.Y., Hu, R.Z., Jiang, S.Y., Li, W.C., Wang, R.C., Wang, D.H., Qi, T., Qin, K.Z., Wen, H.J., 2019. Critical metal mineral resources: current research status and scientific issues. Sci. Found. China 2, 106–111 (in Chinese with English abstract).
Zhang, C.L., Santosh, M., Zou, H.B., Li, H.K., Huang, W., 2013. The Fuchuan ophiolite in Jiangnan Orogen: Geochemistry, zircon U-Pb geochronology, Hf isotope and implications for the Neoproterozoic assembly of South China. Lithos 179, 263–274.
Zhao, G.C., 2015. Jiangnan orogen in South China: developing from divergent double subduction. Gondwana Res. 27, 1173–1180.
Zhao, G.C., Cawood, P.A., 2012. Precambrian Geology of China. Precamb. Res. 222–223, 13–54.
Zhao, J.H., Zhou, M.F., 2013. Neoproterozoic high-Mg basalts formed by melting of ambient mantle in south China. Precamb. Res. 233, 193–205.
Zhao, J.H., Zhou, M.F., Yan, D.P., Zheng, J.P., Li, J.W., 2011. Reappraisal of the ages of Neoproterozoic strata in South China: no connection with the Grenvillian orogeny. Geology 39 (4), 299–304.
Zhao, J.H., Zhou, M.F., Zheng, J.P., 2013. Constraints from zircon U-Pb ages, O and Hf isotopic compositions on the origin of Neoproterozoic peraluminous granitoids from the Jiangnan Fold Belt, South China. Contrib. Mineral. Petrol. 166, 1505–1519.
Zhao, J.Y., Zhang, H., Tang, Y., Lv, Z.H., Chen, Y., 2017. Ore-forming elements diffusion and distribution in the altered host rock surrounding the Koktokay No. 3 pegmatite in the Chinese Altay. Acta Geochim 36 (2), 151–165.
Zheng, Y.F., Zhang, S.B., Zhao, Z.F., Wu, Y.B., Li, X.H., Li, Z.X., Wu, F.Y., 2007. Contrasting zircon Hf and O isotopes in the two episodes of Neoproterozoic granitoids in South China: implications for growth and reworking of continental crust. Lithos 96, 127–150.
Zheng, Y.F., Wu, R.X., Wu, Y.B., Zhang, S.B., Yuan, H.L., Wu, F.Y., 2008. Rift melting of juvenile arc-derived crust: geochemical evidence from Neoproterozoic volcanic and granitic rocks in the Jiangnan Orogen, South China. Precamb. Res. 163, 351–383.
Zhou, J.C., Wang, X.L., Qiu, J.S., 2009. Geochronology of Neoproterozoic mafic rocks and sandstones from northeastern Guizhou, South China: coeval arc magmatism and sedimentation. Precamb. Res. 170 (1–2), 27–42.